COAST 3D

Validation of PISCES Using Data From Teignmouth Pilot Experiment

L.J. Hall
J. Sutherland
J.V. Baugh
T.J. Chesher

Report TR 112
November 2000

EC MAST Project No. MAS3-CT97-0086

HR Wallingford

Validation of PISCES using data from Teignmouth Pilot Experiment

L J Hall
J Sutherland
J V Baugh
T J Chesher

Report TR 112
November 2000

HR Wallingford

Address and Registered Office: HR Wallingford Ltd. **Howbery Park, Wallingford, OXON OX10 8BA**
Tel: +44 (0) 1491 835381 Fax: +44 (0) 1491 832233

Contract

This modelling was carried out as part of the European Community funded Marine, Science and Technology (MAST III) project coastal study of COAST3D. The modelling used field data collected as part of the same project at Teignmouth, UK, during March 1999.

The modelling was carried out within HR Wallingford Ltd by LJ Hall, JV Baugh and TJ Chesher, supervised by Dr J Sutherland. The HR Job numbers were IAS0219 and CNS0037.

Prepared by .....

(name)

.....

(Title)

Approved by .....

(name)

.....

(Title)

Authorised by .....

(name)

.....

(Title)

Date .....

Summary

Validation of PISCES using data from Teignmouth Pilot Experiment

L J Hall
J Sutherland
J V Baugh
T J Chesher

Report TR 112
November 2000

This report describes the application of the HR Wallingford model, PISCES to the Pilot Experiment at the COAST3D site at Teignmouth, UK. PISCES was used to simulate conditions measured during the Teignmouth Pilot experiment, in which an extensive array of wave and current meters was deployed around the seaward side of the mouth of the Teign Estuary. The modelled site is complex, with a headland and an estuary producing strong flows through the estuary mouth. PISCES was used to model a spring tide with no waves, a near-neap tide during a storm and a wave-only case.

The main features of the observed flows were modelled well by PISCES. The water levels in the sea were determined accurately. Water levels in the estuary were modelled well at high tide but were too high in the model at low tide. This result was better for the spring tide than the neap tide with a storm. Most of the irregularities in the currents were also modelled well except for some transient velocity pulses. The spring tide simulation showed vortices being shed from the strong jet-like outflow of the estuary near the middle of the falling tide. These tied in with transient velocity pulses at the fixed metering station that may be a consequence of such features. The modelling of currents during the spring tide was better than the modelling during the neap tide with waves. The near-neap tide during a storm produced relatively high waves and low modelled current, contrasting with the single spring tide. At high and low tide the flow patterns are closer to the wave-only case than the spring tide case. At mid falling tide the strong estuary outflow plays a larger role. The effect of wave breaking is to increase the predicted flow velocities within the surf zone.

The first steps towards compiling an objective set of model validation parameters have been taken by summarising available methods for comparing model performance. The Brier Skill Score provides a measure of mean, phase and amplitude error and involves comparing to a baseline prediction. Its use is recommended because it compares results with those from a baseline model. However, the choice of baseline model should be clearly stated. The model performance statistics confirm that PISCES successfully models the complex flow patterns around this highly three-dimensional site.

Contents

Contents continued

Figures

Appendices

1. INTRODUCTION

This report describes the application of the HR Wallingford model, PISCES to the UK COAST3D site at Teignmouth (Soulsby 1998, 2000) to simulate conditions measured during the Teignmouth Pilot experiment. One of the aims of the project was to use extensive datasets to validate coastal area models. Three test cases have been completed. To this end 19 instruments were distributed over an area of 1.25km by 1.25km around the mouth of the Teign estuary. A variety of instruments were deployed to measure primarily waves, currents and suspended sediment concentration. A subset of the available data was used in this model validation exercise (see Table 2). Detailed bathymetric surveys were made to ensure accurate model grids.

The Pilot Experiment took place from 01 March to 26 March 1999. This experiment was used to test the instrumentation logistics, data analysis procedures and numerical modelling capabilities of the COAST3D partners. It was followed by a more extensive Main Experiment in October and November 1999, when a greater number of instruments were deployed. Details of HR Wallingford's measurements at Teignmouth can be found in Whitehouse et al (2000). HR Wallingford has modelled a 2 week time series from the Main Experiment. Details of this modelling exercise will be included in a subsequent HR Wallingford TR report.

Three test cases from the Pilot Experiment have been completed by the COAST3D modelling institutions:

1 Modelling of a single spring tide with no waves
2 Modelling of a storm waves condition with no tidal flow
3 Modelling of a neap tide with storm waves.

Depth-averaged current vectors and sediment transport vectors were output over the measurement area, through the tides and compiled into animations. Time series of water levels and currents were also compared to measurements.

Model performance statistics were derived and used with the single spring tide to illustrate the model's performance.

2. MODEL SET-UP AND CALIBRATION

PISCES is a state-of-the-art, fully-interactive coastal area modelling framework, capable of simulating the various processes of wave propagation, current distribution, and the resulting sediment transport in complex coastal areas.

For this study PISCES comprised of HR Wallingford's wave propagation model, FDWAVE in combination with the finite element flow model TELEMAC, developed by LNH, Paris and the SANDFLOW sand transport model developed by HR. The models are described in more detail in appendices 1, 2 and 3. A typical application of PISCES comprises of setting up a bathymetric database, selection of specific input wave conditions for simulation, calculating the corresponding currents and sand transport pathways and analysing the results. A consequence of detailed model resolution and sophistication of the models is that it is not usually possible to model all wave conditions in a particular climate, and in any event this would not be a practical option since the sequence of wave conditions is not normally known. Accordingly, PISCES is commonly used to model representative patterns of drift for a selection of waves and the results are integrated to yield the gross and net longshore drift. HR Wallingford has considerable experience in the selection of wave conditions to be representative of this total littoral drift. However, in this case the short-term variations of wave and current climate have been measured and are used in one of the test cases.

This chapter describes the set-up and calibration of the model at the Teignmouth Experiment site. Further details of the TELEMAC flow model, FDWAVE and SANDFLOW are provided in appendices 1 to 3.

2.1 Bathymetry data sources

Data from the bathymetric survey made during the Teignmouth pilot experiment on March 13 1999 and June 1998 was used. Data for the Teignmouth Estuary as far as the tidal limit was digitised from Nunny Survey chart from 1970. Data for beyond the measurement area of the pilot experiment was digitised from Admiralty Chart 3155. All data was combined into a single database for input to each model. Bathymetry was specified relative to Admiralty Chart Datum (ACD) Teignmouth Approaches, which is 2.65m below Ordnance Datum Newlyn (ODN).

2.2 Flow Model Mesh Generation

A finite element mesh of triangles was set up as shown in Figures 1 and 2. The model elements were concentrated in the region of the model where the bed level was above the 5m depth contour and spread more sparsely toward the offshore boundaries. The detailed mesh area had a grid size of around 20m increasing to 250m offshore.

2.3 Flow Model Boundary Conditions and Parameter Settings

For the purposes of the study, a common set of boundary conditions was used by HR and the other modelling institutions. The final choice of boundary conditions involved using water level and north and east component current magnitudes supplied by Delft Hydraulics from their regional model (Ormondt, 2000) for thirteen points around the HR offshore model boundary. The use of their results is acknowledged. The model was driven by a water level boundary at the southern boundary and by flow boundaries at the offshore and northern boundaries. A discharge boundary was specified at the upstream end of the estuary to account for river flow into the estuary. Various boundary relaxation techniques were adopted to achieve a good comparison between the water levels measured by tide gauges during the pilot experiment and those predicted by the model. The parameter settings used are given in Table 1.

Table 1 Parameter settings for TELEMAC flow model

Parameter	Value
timestep	5s
law of bottom friction	Nikuradse's Law
roughness length (k_s)	0.1m
friction enhancement due to waves	yes
turbulence modelling	constant viscosity
velocity diffusivity	2.0m^2/s

It was acknowledged that the roughness length (k_s) should vary over the model domain, but it had been agreed that all modelling institutions would use a constant length throughout their model areas.

The flow model was run through two tidal cycles prior to the actual tidal cycle for which results are required. This is to allow any transients to be removed from the model domain prior to the tide used for comparison.

2.4 Wave Model Set Up

FDWAVE operates on a square grid, which is derived from the TELEMAC mesh at run time. The grid origin is at 296000mE, 67600mN with a grid orientation of 292 degrees from North. The grid size is 20m and extends for 300 grid points in the x-direction and 190 grid points in the y-direction. FDWAVE outputs values of wave breaking stress, wave orbital velocity and wave height onto the TELEMAC grid, so that these can be incorporated into the flow model.

2.5 Combining the Wave and Flow Model

At the beginning of a model run which incorporates wave-driven currents and tidally driven currents, the wave model is first run at the initial water level with still water. The wave model then passes its outputs of breaking stress and wave orbital velocity to the flow model. The flow model then runs through fifteen minutes of the tide. Control then passes back to the wave model that recalculates the wave conditions at the new water level. This is continued through 3 tidal cycles until the flow model had finished. By this means accurate wave propagation is simulated for varying tidal water level (including water level setup at the coast) resulting in accurate combined wave-driven and tidal currents.

2.6 Sediment transport

Sediment transport under combined waves and currents is calculated with the HR Wallingford sand transport model SANDFLOW. The wave and tidal induced flows that are output from TELEMAC and the wave orbital velocities output from FDWAVE are used to determine the total load transport. SANDFLOW solves an advection-diffusion equation for the concentration of sand. For most applications the suspended load fraction is greater than the bed load transport and hence this approach is valid.

It is acknowledged that the site is characterised by mixed sediment varying from gravels to fine sand and mud in the estuary. However, for the purposes of the initial investigation transport of sand of grain size 0.15mm was simulated. The consequence of spatially varying deposits is an item for consideration as part of the full model studies.

3. FIELD DATA

Teignmouth is located on the south coast of England. The area is very three-dimensional with an estuary mouth and a rocky headland all adjacent to the beach, with its sea defences. The Pilot experiment at Teignmouth ran for a period of 4 weeks from 1 March to 26 March. The experiment was set up on the basis of three main transects to examine the cross-shore and long-shore processes and gradients in processes and to provide data for model validation. The locations of all the instruments deployed in the pilot are shown in Figure 3. The two cross-shore transects (north and south) form the basis of two contrasting linear arrays, one in the relatively open coast to the north and the other in the area where the 3D effects are expected to be greatest. The shore-parallel East transect is added to provide information in the alongshore direction. The data available from the pilot experiment for the present study is listed in Table 2. Locations are given by OS coordinates and by a number used in Figure 3 to show where the instruments are. In Table 2 pt = pressure transducer, cm = current meter, ADP = acoustic doppler profier and wr = waverider buoy. A description of the waves and water levels during the Pilot Experiment is given in Appendix 4.

Table 2 Equipment used in model verification at Teignmouth

Location number	Location mE, mN	Instrument	Data type	Data rate (No per hour)
4	294705, 72668	pt	waves	1
6	295183, 72357	pt, cm	waves and currents	1
8	294347, 72656	pt	water level	6
11	293885,72696	pt	water level	6
14	294298,72445	pt, cm	waves and currents	1
18A	294373,72374	pt, cm	waves and currents	1
24A	294243,72319	pt, cm	currents	1
25	294678,71914	pt, cm	directional waves and currents	1
26	294834,71811	ADP, wr	waves and currents	1,2
32	294076,71556	pt, cm	waves and currents	1
33	294493,71281	pt, cm	waves and currents	1

3.1 Burst numbers

Within COAST3D all dates and times are represented by burst numbers. The burst number is the number of hours since the start of the COAST3D project, so burst 1 is at 01:00GMT on 1 October 1997, burst 2 is at 02:00GMT on 1 October 1997, etc. Examples of burst numbers from the Teignmouth Pilot experiment are shown in Table 3. The number of minutes after the hour is denoted by the subburst number. All times are in GMT.

Table 3 Examples of burst numbers at Teignmouth

Date	Time	Burst number	Comment
01/10/97	01:00	1	Day 1 of COAST3D
08/03/99	12:00	12564	Mon, week 1, Teignmouth Pilot
10/03/99	12:00	12612	Wed, week 1, Teignmouth Pilot
12/03/99	12:00	12660	Fri, week 1, Teignmouth Pilot
14/03/99	12:00	12708	Sun, week 1 Teignmouth Pilot
16/03/99	12:00	12756	Tue, week 2 Teignmouth Pilot
18/03/99	12:00	12804	Th, week 2 Teignmouth Pilot
20/03/99	12:00	12852	Sat, week 2 Teignmouth Pilot
22/03/99	12:00	12900	Mon, week 3 Teignmouth Pilot
24/03/99	12:00	12948	Wed, week 3 Teignmouth Pilot
26/03/99	12:00	12996	Fri, week 3, Teignmouth Pilot

4. SINGLE SPRING TIDE (NO WAVES)

In order to simulate conditions dominated by tidal action, a large spring tide with low wave conditions was modelled from 08:10 GMT on 20/03/99 (burst 12848, sub burst 10) to 20:40 GMT on 20/03/99 (burst 12860, subburst 40), a total length of 12 hours 30 minutes.

Depth-averaged tidal currents, given in north and east components, and water levels were output at ten minute intervals from the flow model. From the sediment transport model, north and east components of sediment flux were output at fifteen minute intervals. This test case was also repeated with a lower viscosity of 0.5 (rather than 2.0 as used in the main run) to see if more vortices were shed.

Figures 4 to 7 show current and sediment transport vector plots at four instances during this tidal cycle; high tide, mid (falling) tide, low tide and mid (rising) tide respectively. An animation of the whole tide has also been made. At high tide (Figure 4) the offshore tidal flow to the North can be seen. There is still some flow into the estuary and small vortices can be seen immediately to the North of the Ness and in the estuary behind the tip of the point (North side of estuary). There is effectively no sediment transport at this time. By mid (falling) tide (Figure 5) the flow is dominated by outflow from the estuary. Within the estuary the flow follows the 2 main channels around the top of the Salty, which has started to dry out. These flows converge at the mouth of the estuary, emerging as a strong jet current. A large vortex has been shed to the South of the main flow but there is (in Figure 5) no vortex shed to the North of the jet. Sediment transport is dominated by the flow down the main channels of the estuary and the jet emerging from it where the sediment transport rates exceed 1kg/m/s. Note, however, that the bed in those areas is assumed to be fine sand in the model whereas, if fact, the bed in these areas consists of larger material. The strong current will soon move any sand that is deposited in the main channel, as shown by the model.

At low tide (Figure 6) the tidal flow to the south can be seen offshore. There is still some outflow from the estuary as the water level within the estuary is higher than in the open sea (as shown by Figure 8). Within the estuary the flow is mainly down the deepest channel to the North of the estuary. A large area of the Salty and the beach to the North of the estuary, including Spratt sand, has dried out. On emerging from the estuary the flow splits into 3 jets, following the 3 deepest channels past the sand banks. Vortices are again

formed mainly to the South of the main jet. Sediment transport is again dominated by the main jet flow. By mid (rising) tide (Figure 7) there is a stronger tidal flow offshore than at mid (falling) tide (compare Figures 5 and 7). Moreover, the flow into the estuary is more evenly spread (less jet-like, with lower gradients in flow speed) and there is no vortex shedding at the edges of the main flow. There is some sediment transport over Spratt Sand as well as in the main channels as there are quite high flow speeds there.

Figure 8 shows the tidal residual depth-averaged sediment transport rate and the changes in bed level (averaged over the whole tidal cycle). There is a divergence in the sediment transport rate at the mouth of the estuary where the bed level reduction simulated is over 0.5m in some places. The run assumes a constant grain size throughout the model area. In practice there are larger grain sizes in some areas, especially around the mouth of the estuary and over the Salty which has established weed on it. The model predicts deposition in the region of the sandbanks around the mouth of the estuary. The model run shows that any sand that is deposited in the mouth of the estuary will soon be moved away, so maintaining the deep channel at the estuary mouth, but reinforcing the sandbanks further offshore (hence the need for dredging to maintain the navigation channel).

Figure 9 shows a comparison between water levels given by the model and those measured at locations 8 and 11 (the tide gauges in the open sea and the estuary respectively). The water levels at tide gauge 8 are well represented, as are the levels at tide gauge 11, except near low water when the water levels do not fall low enough. This may be due to using a constant roughness that is not representative of conditions in the estuary, or due to using the somewhat old bathymetry data for the estuary. The problem indicated the difficulty in modelling flow from and over extensive areas of sand banks and mud flats.

Figures 10 and 11 show comparisons between velocities measured at a point in the field and the depth-averaged currents predicted by the model. The use of lower viscosity did not give any improvement in the model results compared to the field data, although it allowed more vortices to develop. Locations 6, 32 and 33 are on the edges of the experimental box. Their positions are shown in Figure 3 and the box outline in Figures 4 to 7. Their results are in Figure 10. The currents are well represented throughout the tidal cycle except at location 6 for the period from burst 12850 to 12852. The measurements can be interpreted as showing a large vortex passing that point after being shed from the main jet during the falling tide. PISCES did not predict a vortex extending that far from the main jet. Locations 25, 18, 24a and 14 (Figure 11) are within the experimental area (Figure 3). Location 25 is quite close to the offshore edge of the box while 24a, 18a and 14 are on East Pole Sand. The currents are generally well predicted especially at 24a where the rapid variations in the falling tidal currents are accurately represented. Small errors in predicting the size, strength and position of shed vortices can lead to quite large relative errors in the current predictions, which may explain some of the discrepancies.

4.1 Discussion of Spring Tide Modelling

A qualitative assessment of PISCES modelling of a single spring tide is provided below. A quantitative assessment of the current modelling is provided in Section 8 through the use of a number of model performance statistics.

Water levels in the open sea are represented well in the model throughout the tide. Water levels in the estuary are also modelled well except near low tide, illustrating the difficulty in modelling flow over sand banks and mud flats. The complex three dimensional nature of the site resulted in irregular measured time series of velocities (Figures 10 and 11). These currents were also modelled well with most of the irregular features reproduced accurately. Some of the strong transient flow features that occurred during the following tide were not reproduced in the model. These can be interpreted as vortices passing the measurement locations. The model does show vortices shed from the jet-like outflow from the estuary. However, small errors in predicting the vortices can lead to large relative errors in the current at a po int. The model reproduces some, but not all of the vortices correctly.

A uniform grain size was used throughout the model area by all COAST3D modelling institutions for this common test case. This proved to be an unrealistic choice due to the large diversity of grain sizes in the model area. Large bed level changes were predicted at the mouth of the estuary where the measured grain size was a lot larger than the size in the model. This emphasises the need to run these models using different characteristics for different areas.

5. SINGLE WAVE CONDITION

The second test case was a no-flow situation with a single wave condition. Note that stipulating that there are no currents (except those driven by the waves) makes this an unrealistic case as there is always some tidally driven flow in the test area. Nevertheless, it is an interesting test case as model predictions at a complex site can be studied. The conditions modelled were:

- Wave height H_s= 1.8m, converted to H_{rms} by dividing by √2.
- Mean wave period (Tz) = 5s
- Wave direction = 120 degrees north
- Fixed water level = 3.04m ACD
- Sediment size and bed roughness data: As above

For this case the waves was run over the model area for a period of three hours after which the wave induced currents reached equilibrium. Wave heights and periods, wave orbital velocities, breaking stresses and wave-induced currents were used to calculate sediment transport rates due to this wave condition. Figure 12 shows the significant wave heights and vectors of wave orbital velocities as predicted by the model. The wave orbital velocity vectors show the effects of refraction and wave breaking near the shoreline. Figure 13 shows vectors of the wave-induced currents and the resulting sediment transport. There is a complicated pattern of wave-induced currents (quite unlike the tidal currents in Figures 4 to 7) including a series of vortices along the coast. The strongest currents and sediment transport rates are over the top of East Pole Sand where intense wave breaking occurred. The waves are also generating currents into the estuary.

5.1 Discussion of wave-only case

A qualitative discussion is all that is possible here as there is never a time when there are no tidal flows and no flow into or out of the estuary. The results look reasonable with the greatest wave induced currents occurring where the breaking is strongest. The predicted flow pattern is quite different from the spring tide flow pattern. An interesting feature is that onshore sand transport is predicted over East Pole Sand for this wave condition.

6. NEAR-NEAP TIDE PLUS WAVES AT PEAK OF STORM

A storm with maximum offshore wave height about 1.9m occurred at the start of the pilot experiment, close to a neap tide. This represents a case with relatively high waves and low tidal currents. Results were output from 23:00 GMT on 10/03/99 (burst 12623 subburst 00) to 11:00 GMT on 11/03/99 (burst 12635 subburst 30), a total length of 12 hours 30 minutes. The flow model was run 3 times with tidal conditions plus:

I. No waves
II. A constant wave condition, with wave height, period and direction the same as for section 5.
III. Time-varying wave height, period and direction as given at hourly intervals by the measured data.

The sediment size and Nikuradse roughness were as before (Section 2). Depth averaged tidal currents, given in north and east components, and water levels were output at ten-minute intervals from the flow model. From the sediment transport model, north and east components of sediment flux were output at fifteen-minute intervals.

Figures 14, 15, 16 and 17 show water depth, depth-averaged (tidal and wave-induced) currents and depth-averaged sediment transport rates at 4 stages during the tide: high tide, mid (falling) tide, low tide and mid (rising) tide respectively. The results are from run III, with time varying waves. At high tide (Figure 14) there are tidal flows offshore and wave-induced flows in shallow water, with an area of lower currents in between. The flow pattern is more similar to the wave only case (Figure 13) than the spring-tide (no wave) case (Figure 4). For example, there is a anti- clockwise-rotating vortex over Spratt Sand and a clockwise-rotation to the North of East Pole Sand. The flow speeds are lower than for the wave-only case. By mid (falling) tide (Figure 15) the flow speeds had increased and the current and sediment transport vectors are similar to those from the wave-only case (Figure 13). There is, however, a large flow out of the estuary which increases the northward flow along the edge of East Pole Sand and forces a smaller jet south-east from the Ness, creating stronger vortices there.

At low tide (Figure 16) there is a southerly flow offshore which interacts with the estuary outflow to produce a large vortex, the centre of which is close to location 6 on the edge of the measurement box. Some very large sediment transport vectors are calculated in shallow water (less than 2m depth). The area of sediment transport extends further offshore than in the tidal current only case. By mid (rising) tide (Figure 17) there is flow into the estuary and the centre of the large vortex (on the North side of the flow into the estuary) has moved south-west, back into the measurement box. The main offshore flow is to the South.

Figure 18 shows a comparison of modelled and measured water levels at the two tide gauges and reveals that the estuary does not empty enough in this case. The comparison is not as good as that for the spring tide case (Figure 9). This may again be due to using a constant roughness that is not representative of conditions in the estuary, or rather old bathymetry data for the estuary. Alternatively it may be partly caused by the action of the waves in a similar way to the wave-only case (Figure 13) where water is held in the estuary by the waves.

Figures 19 and 20 shows comparisons between the predicted depth-averaged currents from runs I, II and III and the point measurements. The measurement positions are shown in Figure 3 and the box outline is in Figures 14 to 17. Locations 6, 32 and 33 are on the edges of the experimental box and the currents through the tide are shown in Figure 19. The tidal velocities are generally low (less than 0.2m/s) and the predictions are smoother than the measured time series. The small spikes in velocity at location 6 during burst 12626 and at location 32 during burst 12629 are not well represented. This may imply that the model is not shedding vortices correctly. The differences between the 3 model runs are low and none appears to be significantly better than the others. All 3 points are outside the normal surf zone so the waves should only have a small effect.

Locations 25, 18a, 24a and 14 are within the experimental box and the currents through the tide are shown in Figure 20. The currents are low at location 25 (near the offshore edge of the experimental box). The current speeds at location 18a are much higher than further offshore especially near low tide (note the change in scale between Figures 19 and 20). This is due to heavy wave breaking when the water depth is lower. The model prediction with no waves gives a low current speed, showing the importance of wave breaking in driving currents here. The predicted currents from the model runs with changing waves and a constant wave are similar. They predict the magnitude but not the direction of the high currents around 04:00 GMT to 07:00 GMT (bursts 12628 to 12631) reasonably well. Figures 16 and 17 show the complicated current pattern during this time. A small shift in the position of the centre of the vortex would lead to large shifts in the direction of the current at location 18a as it is quite close to the centre of the predicted vortex. Both measured and predicted currents are substantially lower at locations 24a and 14 than at 18a. (18a and 14 are only about 100m apart while 18a and 24a are about 150m apart.) The magnitude, but not the direction, of the peak current at location 14 between 0400 and 0500 GMT (during burst 12628) is reasonably well represented by model runs II and III.

6.1 Discussion of neap tide plus storm modelling

The model reproduced water level variations at location 8 accurately. The model predictions for water level at location 11 (in the estuary) were not as good as for the spring tide case. The reasons are likely to include those discussed in the spring tide case plus the effect of the wave model in holding water in the estuary.

Currents outside the surf zone (at locations 6, 25, 32, 33) are not quite so well represented here as for the spring tide case. In particular the small variations (lasting the order of 1 hour) are not all reproduced. Current speeds are very low, however, so small fluctuations from the measurements are unlikely to have a significant impact. The difference in current speeds caused by adding a wave model is normally less than $0.1 ms^{-1}$ at locations 6, 25, 32 and 33.

There are only 3 measurement locations that are within the surf zone for most of this test. They are locations 14, 18a and 24a. Mode runs II and III (with waves) produced current speeds that were up to $0.6 ms^{-1}$ greater than model run I (no waves). The measured current speeds were much higher at 18a than for the spring tide case.

PISCES was able to reproduce some, but not all of the measured flow features during the neap tide with storm waves case. Magnitudes of peak flows were reproduced better than directions. A greater number of measurement points (in space and time) would be needed before definite conclusions could be reached. However, run II (using a constant wave condition) appeared to do as well as run III (using a wave condition that varied each hour). Updating the wave condition each hour does not appear to be necessary.

The modelled currents are significantly changed by the wave-breaking induced currents. These can be altered by variations in wave direction and the choice of wave breaking criteria used. Sensitivity tests could be run to determine whether a better combination of parameters exists.

7. MODEL PERFORMANCE STATISTICS

The question of how good a model is can be defined in a more quantitative manner than the usual qualitative ranking that is normally applied. Model Performance Statistics (MPSs) provides a means of comparing model performance to data. Note, however, that it is not possible to make any objective conclusions without a discussion of the measurements and their inherent errors. Moreover, the degree of model tuning will play a role in determining the goodness of fit. The following sections sumarise the available statistical tests.

7.1 Closeness of means and variances

Suppose that there is a set of measured values and a corresponding set of model values. These could be time series of wave height, current speed or current direction at a point or they could be a set of results from a number of spatially separated gauges from the same time. Let X_n be the measured value and Y_n be the model output value, with $n = 0, \ldots, N$. Sometimes $n=0$ is the initial or offshore boundary value used to drive model (so in this case $X_0 = Y_0$).

The simplest statistics to compare are the mean and variance of sets of modelled and measured data. A common test to see whether the difference between 2 means is significant or not is the Student's t test which looks at the difference in standard errors. Typically the standard error is equal to the sample's standard deviation divided by the square root of the number of points in the sample. However much of the variance in both samples will normally be caused by effects (such as the rising and falling tide) that are common to both samples. For example the mean tidal residual current at a point will often be small but the variance can be quite large as the current varies through the tide. This large variance will decrease the statistical significance of any difference between the measured and modelled mean (tidal residual) current.

To minimise this problem the following analysis may be performed with the paired samples. The covariance between the two sets of results is calculated as:

$$\mathrm{Cov}(X,Y)=\frac{1}{N}\sum_{i=0}^{N}(X_i'Y_i') \tag{1}$$

with $X_i' = X_i - \langle X \rangle$ and ⟨X⟩ the average of X. Similarly for Y. Then the standard error becomes:

$$s_D = \left[\frac{\sigma^2(X)+\sigma^2(Y)-2\mathrm{Cov}(X,Y)}{N+1}\right]^{1/2} \tag{2}$$

with $\sigma^2(X)$ the variance in X and the t-statistic is given by:

$$t = \frac{\langle X \rangle - \langle Y \rangle}{s_D} \tag{3}$$

The significance of the t-statistic is calculated for $\nu = N$ degrees of freedom by calculating the probability $A(t/\nu)$ that t would be smaller than the calculated t if the means are the same. The two means are significantly different when A is close to 1. If the means are identical then $t = 0$ and $A(0/\nu) = 0$. In general:

$$A\left(\frac{t}{\nu}\right) = 1 - I_{\frac{\nu}{\nu+t^2}}\left(\frac{\nu}{2},\frac{1}{2}\right) \tag{4}$$

where $I_x(a,b)$ is the incomplete beta function.

The F-test can be used to determine whether the 2 sets of numbers have significantly different variances. Again assume paired sets of data (although the test may be generalised for sets of different length). Let F be the ratio of the 2 variances σ^2 (X) and σ^2 (Y), the larger divided by the smaller. Then the data sets have different variances for large or small values of F. The probability that the variances are the same is given by:

$$Q = 2I_{1/(1+F)}\left(\frac{N}{2},\frac{N}{2}\right) \tag{5}$$

If Q is greater than 1, take 2-Q as the probability that the variances are the same.

In many cases it may be pertinent to ask whether the modelled and measured data come from the same distribution (see Press at all). The measured and modelled data will be treated as coming from unknown distributions. The data can be binned or continuous and any continuous dataset may be sorted into bins. The disadvantage of binning a continuous dataset is that a lot of information is lost. The advantage is that it is easy to see what percentage of the model results lies within a certain range of the observations. This is especially valuable where you have an idea of how accurate the measured data is as the ranges can expressed in terms of a number of error bands. For example, if the measured wave height at a point is quoted as being accurate to 0.1m the percentage of modelled wave heights that are within ±0.1m, ±0.2m, ±0.3m, etc of the measured wave heights will be of interest.

7.2 Linear and rank order correlation

The most widely used method of determining whether 2 time series are related is the linear correlation coefficient, r_{XY} given by:

$$r_{XY} = \frac{\langle X'Y' \rangle}{\sigma(X)\sigma(Y)} \tag{6}$$

The value r_{XY} = 1denotes complete positive correlation while r = 0 occurs when X and Y are uncorrelated. The coefficient r is a measure of how strong a correlation is but not how significant the correlation is because the distributions of *X* and *Y* are not taken into account. If both distributions converge sufficiently and N is large (Press et all suggest N > 500) then the 2 distributions are significantly correlated when there is a small value of the complementary error function $\mathrm{erfc}\left(|r|\sqrt{(N-1)/2}\right)$. Further assumptions lead to statistics for small sets of data (N << 500 as is commonly the case in coastal engineering). The correlation coefficient takes into account errors in amplitude and phase, but not errors in the mean value. Nor does it take into account the initial condition or any baseline prediction. Note, however, that if $G_n = aY_n+b$ for all *n* then $r_{XY} = r_{XG}$.

The assumptions about the distributions of *X* and *Y* in the calculation of the significance of the correlation can be avoided by calculating a nonparametric or rank correlation. To do this, sort the time series of data into ascending (rank) order. In cases where the same number occurs more than once ascribe the mean value of the ranks they would have had had they been slightly different to all the equal numbers. Although information is lost by this procedure, the significance of the correlation can be calculated without needing to know the distributions of X and Y.

Let R_i be the rank of X_i among the *N+1* values of *X*. Moreover, let $R_i' = R_i - \langle R \rangle$ and $\sigma^2(R)$ be the variance in *R*. Similarly let S_i be the rank of Y_i among the N+1 values of *Y*, $S_i' = S_i - \langle S \rangle$ and $\sigma^2(S)$ be the variance in S. The rank order correlation is the linear correlation coefficient of the ranks:

$$r_s = \frac{\langle R'S' \rangle}{\sigma(R)\sigma(S)} \tag{7}$$

The significance of r_s values above zero is obtained by first computing the t-statistic:

$$t = r_s \sqrt{\frac{N-1}{1-r_s^2}} \tag{8}$$

which is approximately a Student's t distribution with N-1 degrees of freedom. The significance is then given by $A(t/\nu)$. A large value of $A(t/\nu)$ indicates a large significance.

Sutherland and O'Donoghue (1997) have used the rank order correlation between predicted and measured time series of cross-shore horizontal velocity to assess the accuracy of a mathematical model of wave reflections from structures. In this case long time series (of 4096 points) were used to calculate the correlation. Moreover the wave field (in the UK Coastal Research Facility) was stationary throughout the test. In cases where much smaller sets of data have been gathered (or where model results are scarce) other statistics have been used, especially where the data is a mixture of a few points in space and a few in time.

7.3 Performance indices from wave model validations

Zambresky (1989) conducted a verification study of the global WAM model, which involved comparing time series of statistics measured at offshore buoys to time series of model parameters. The compared statistics were:

- Mean value and bias (difference of means)
- Standard deviation
- Root mean square error (plus systematic and unsystematic rms error defined using the slope and intercept of a least-squares regression)
- Linear correlation coefficient
- Scatter Index (SI) which is the rms difference (between modelled and measured values) divided by the average measured value

$$SI = \frac{\sqrt{\left\langle (X_n - Y_n)^2 \right\rangle}}{\langle X \rangle} = \frac{\text{rms}_{difference}}{\langle X \rangle} \tag{9}$$

Three model performance statistics were used in a recent paper (Ris et al 1999) aimed at verifying the performance of the coastal area wave model, SWAN. They are:

- Scatter Index (SI) from Zambresky
- Operational performance index (OPI) which is the rms difference divided by incident observed value, X_0

  $$OPI = \frac{\sqrt{\left\langle (X_n - Y_n)^2 \right\rangle}}{X_0} = \frac{\text{rms}_{difference}}{X_0}. \tag{10}$$

  OPI values tend to be low (at least for wave height) as X_0 values are high.
- The Model Performance Index, MPI, was defined in terms of rms difference and rms changes (difference between X_n and X_0)

  $$MPI = 1 - \frac{\sqrt{\left\langle (X_n - Y_n)^2 \right\rangle}}{\sqrt{\left\langle (X_n - X_0)^2 \right\rangle}} = 1 - \frac{\text{rms}_{difference}}{\text{rms}_{change}} \tag{11}$$

In the cases considered by Ris et al (1999) the X_n and Y_n are the measured and modelled significant wave heights or wave periods at a number of buoys at the same time, with X_0 the offshore wave height (or period) used to drive the model so $X_0 = Y_0$. X_0 is omitted from the averaging of the X_n values. Note that the rms difference between the modelled and measured values is due in part to the errors in the measurements as well as to the errors in the modelling. Low values of SI indicate a good model performance. However, the SI can become quite high where the average measured value is low, which is quite often the case for coastal engineering, but is less of a problem offshore where the statistic was derived.

Consider the contrasting cases of a set of wave height measurements made outside the surf zone and another set made over the inner bar of a double-barred beach for the same offshore wave conditions. If the rms error in wave height in both cases is 0.25m but the average wave height is 5.25m offshore, 5m just outside the surfzone and 1m over the inner bar then the respective scatter index values are 0.05 and 0.25. The second case is much more complicated to model than the first and the rms error is no worse than in the first case yet the SI gives a much worse value for this case. OPI values tend to be low (at least for wave height) as X_0 values are high. Its failing is therefore the same type as the Scatter Index. In the fictitious example used for the SI, the OPI values offshore and over the inner bar are both 0.048.

For a perfect model and a perfect dataset, the MPI = 1 as $\text{rms}_{difference} = 0$. If the model predicts no changes, $Y_n = X_0$ so $\text{rms}_{difference} = \text{rms}_{change}$ so MPI=0. Alternatively, if $\text{rms}_{difference}$ is greater than $\text{rms}_{changes}$ then the MPI is negative. Note that the value of the MPI will decrease if the errors in the measurements increase as well as when the model performance worsens. In the fictitious example above, MPI = 0 just outside the surfzone and MPI = 0.95 over the inner bar.

Another form of normalised mean square error is defined as:

$$\text{normalised MSE} = \left\langle \left(\frac{X'}{\sigma(X)} - \frac{Y'}{\sigma(Y)} \right)^2 \right\rangle \tag{12}$$

A perfect agreement has a value of zero but a random discrepancy has a value of 2.

Other options to consider are the minimum and maximum absolute deviation between measured and modelled and measured results and the difference in the means and variances of X and Y. The latter may

be written as the standard error (so that its significance can be determined) or as a model variance index, MVI, given by:

$$\mathrm{MVI} = \frac{\sqrt{\sum_{1}^{N}(Y_n - Y_0)^2}}{\sqrt{\sum_{1}^{N}(X_n - X_0)^2}} = \frac{rms_{\mathrm{model\_change}}}{rms_{change}} \qquad (13)$$

Given that $Y_0 = X_0$, MVI is determined by the rms changes predicted by the model and the rms changes measured. When the model predicts the measured changes the MVI = 1. Note however, that this could occur even when the model does not predict the measured wave height at each point. If the model predicts too much dissipation, for example, the wave height MVI is greater than 1, whereas if it predicts too little dissipation, for example, the wave height MVI is less than 1.

The above indices are easily calculated for scalar quantities. Their application to vector quantities (such as currents) is less obvious. The obvious way is to represent magnitude and direction as 2 separate scalars and consider each independently of the other.

7.4 Brier Skill Score.

Brier Skill Score, *BSS*, is defined in terms of mean-squared differences between measured values, modelled values and a set of baseline predictions, B_n

$$BSS = 1 - \frac{\frac{1}{N}\sum_{1}^{N}(X_n - Y_n)^2}{\frac{1}{N}\sum_{1}^{N}(X_n - B_n)^2} = 1 \qquad (14)$$

The baseline prediction can be original measured bathymetry, with *X* the measured final bathymetry and *Y* the predicted final bathymetry. Alternatively the baseline prediction could be a measure of the average climate (so could be the average measured wave height or current at a point). A skill score of 1 implies perfect modelling, a score of 0 implies that you have done no worse than the baseline prediction and a negative score implies that your model results are worse than the baseline prediction. The BSS reduces skill for mean, phase and amplitude errors.

7.5 Effect of measurement errors on performance statistics

All measurements have a related degree of uncertainty and, in an ideal world, would be quoted with error bars. Errors can arise from the calibration of an instrument or from making assumptions about the values of density, speed of sound, or the elevation of the instrument above the bed in the analysis procedure. In this model validation test case the depth-averaged currents from the model are compared to measurements made at a fixed point, so like is not compared to like. The current at a point can be related to depth-averaged current by assuming a current profile, but this involves an additional assumption.

Errors in the computation of wave statistics can arise from:

(i) not including currents in the solution in the dispersion relationship
(ii) filtering the data incorrectly (especially when there are large pressure attenuation correction factors being used)
(iii) statistical instability due to the random variability of spectral moments
(iv) uncertainty due to the choice of method for spectral estimation
(v) sampling rate errors in time series analysis.

For example, the standard deviation of estimates of peak period are commonly much larger than the standard deviations of estimates of average periods. Van Rijn et al (2000) have produced a report on measurement errors in field conditions for the COAST3D project. Relevant conclusions from that report are:

(i) Time-averaged velocities larger than $0.5ms^{-1}$ have an error less than 15%
(ii) Time-averaged velocities smaller than $0.5ms^{-1}$ have an error less than 30%.
(iii) RMS and significant wave heights in non-breaking conditions have an error of less than 10%
(iv) RMS and significant wave heights in breaking conditions have errors less than 15%.

The presence of measurement errors inevitably reduces the apparent model performance. Statistical tests of uncertainty generally ignore the presence of measurement errors and are of limited use. The quality of modelling associated with a particular value of a performance statistic will depend on the size of the measurement error, the number of points used and the nature of the phenomenon studied.

8. APPLICATION OF MODEL PERFORMANCE STATISTICS TO PISCES MODELLING OF TEIGNMOUTH

The following Model Performance statistics were calculated for velocities during the spring tide case:

- BSS = Brier skill score from measured velocities, modelled velocities and model velocities at the model boundary directly offshore from Teignmouth [equation 14].
- $\langle X \rangle$ = mean of measured velocities [m/s]
- $\langle Y \rangle$ = mean of modelled velocities [m/s]
- PDM = probability that the mean velocities are different [equation 4]
- $\sigma(X)$ = standard deviation of measured velocities [m/s]
- $\sigma(Y)$ = standard deviation of modelled velocities [m/s]
- pvs = probability that variances of velocities are the same [equation 5]
- SI = scatter index = rms difference between velocities divided by mean of measured velocities [equation 9]
- s_D = standard error between measured and predicted velocities [equation 2]
- r_s = Spearman rank order correlation (between measured and predicted velocities) [equation 7]
- r_{XY} = Pearson linear correlation coefficient [equation 6]

The significances of the Pearson and Spearman correlation were also calculated, but as the values were reasonable they are not quoted. The statistics were calculated for velocity time series at locations 6, 33, 14 and 24 using the component of velocity resolved to North (Un) the component of velocity resolved to East (Ue) and the current speed (U). The results are shown in Table 4.

Table 4 Model Performance Statistics from PISCES modelling of Teignmouth Pilot experiment

Vel	**Un**	**Ue**	**U**	**Un**	**Ue**	**U**	**Un**	**Ue**	**U**	**Un**	**Ue**	**U**
Item	**6**	**6**	**6**	**33**	**33**	**33**	**14**	**14**	**14**	**24**	**24**	**24**
BSI	0.36	0.33	0.45	0.83	0.61	0.81	0.87	0.67	0.84	0.78	0.87	0.66
$\langle X \rangle$	0.03	-0.01	0.13	0.06	0.01	0.08	0.03	0.00	0.09	0.03	-0.02	0.19
$\langle Y \rangle$	0.03	0.03	0.14	0.07	0.03	0.10	0.02	-0.01	0.10	0.04	-0.02	0.18
PDM	0.17	1.00	0.98	1.00	1.00	1.00	0.85	0.86	0.67	0.62	0.25	0.57
$\sigma(X)$	0.120	0.056	0.046	0.076	0.032	0.055	0.078	0.063	0.054	0.103	0.173	0.081
$\sigma(Y)$	0.132	0.055	0.042	0.093	0.035	0.083	0.049	0.088	0.041	0.069	0.177	0.069
Pvs	0.386	0.895	0.403	0.061	0.355	0.000	0.000	0.005	0.015	0.001	0.853	0.168
SI	1.92	-6.62	0.46	0.70	8.81	0.55	1.75	-18.49	0.54	2.06	-3.04	0.36
s_D	0.006	0.005	0.006	0.004	0.003	0.005	0.006	0.006	0.006	0.007	0.007	0.008
r_s	0.85	0.80	0.35	0.93	0.69	0.84	0.73	0.78	0.30	0.79	0.92	0.47
r_{XY}	0.91	0.60	0.16	0.94	0.66	0.88	0.72	0.80	0.51	0.82	0.94	0.60

The measured current speed, modelled current speed and baseline prediction of current speed (the model boundary value) are shown in Figure 21 for reference. The Brier Skill Index, Scatter Index, rank order correlation and linear correlation between measured and predicted current speeds are shown in Figure 22. The Brier Skill Score ranges from 0.33 to 0.87 for components of velocity and from 0.45 to 0.84 for current speed. The means are all quite low and the statistical probabilities of the means being different are all quite high. The low means result in some very high Scatter Indices. These are lower (0.36 to 0.55) for the current speed as the average speeds are higher. The correlation coefficients range from 0.30 to 0.92 for the rank order correlation (r_s) and from 0.16 to 0.94 for the linear correlation (r_{XY}). The lowest correlations occur for items 6 and 14 with the largest spikes in the measured data when the jet-like current from the estuary (or vortices shed from it) flows over the instrument.

Figure 22 shows that the model performs quite well in predicting the current speeds. The issue of what sort of value indicates a good result still has to be solved. The value of the Brier Skill Score (or index) depends on the form of the baseline prediction made. Any positive value for the BSS implies an improvement on the baseline prediction. The present work deals with vectors by considering 2 components resolved to North and East as well as the current speed. Methods for treating vectors based on mean absolute differences have also been developed and will be applied to the modelling of Teignmouth Main experiment.

Model performance statistics help to define the ability of a numerical model to reproduce measured phenomena well. Their use will provide some level of objective comparison between models. A reasonable number of tests will have to be done to establish the ranges of the MPSs that can be considered as good modelling. This will, however, vary from site to site and application to application. In the above example the lowest Brier Skill Scores came from the cases where short-lived but strong eddies from the estuary outflow passed over the instruments. These are difficult to model precisely but it may not be necessary to model them precisely in order to be able to model the overall changes in bathymetry, for example. It is nevertheless reasonable to expect a model to perform less well in cases where there are strong, transient features.

Caution must also be applied when comparing statistics between heavily-tuned models and those applied more-or-less blind. Moreover in regions with large spatial gradients model resolution may affect the performance. In areas of rapidly changing conditions it may be found that the average velocity (or wave height) within a model cell does not agree as well with the measured data as the velocity (or wave height) within a neighbouring model cell. This is especially likely to occur when the measurement is made near the edge of a cell.

9. CONCLUSIONS

The HR Wallingford coastal area model PISCES has been applied to the COAST3D project site of Teignmouth in Devon, UK, to simulate conditions measured during the Teignmouth Pilot experiment. The PISCES model comprised 3 modules: the TELEMAC-2D finite element flow model, the FDWAVE wave propagation model and the SANDFLOW sand transport model.

Teignmouth is located on the wouth coast of England on the west side of Lyme Bay. The area is very three dimensional with a large estuary emptying through a narrow mouth, a rocky headland and a groyned beach with sea defences. There is a series of mobile sandbanks offshore of the mouth of the estuary. A complicated circulation pattern results and provides a very severe modelling test.

Three common test cases have been modelled:
1. Spring tide with no waves
2. Single wave condition
3. Near-neap tide plus waves at peak of storm.

The model reproduced the main irregular features of the flow in the spring tide case. The model showed vortices being shed from the strong jet-like outflow from the estuary near the middle of the falling tide. The experimental results also showed the presence of large spikes in velocity that can be interpreted as vortices at the same time during the tidal cycle. The vortices were not modelled perfectly and small errors in predicting the path of the centre of the vortex can lead to large errors in the predicted flow direction and speed. The model did better at predicting vortices to the north of the main jet outflow than to the south. Sediment transport rates and tidal-residual changes to the bathymetry were predicted. Rather large changes to the bed levels were predicted just outside the estuary mouth. This is due to the offshore sediment size ($d_{50} = 0.15$mm) being applied to the whole model domain when, in practice, the sediment size becomes larger in the estuary mouth and up on the beach. All modelling groups in COAST3D applied the same grain size throughout their model areas to allow the models to be compared more easily. Clearly the site is characterised by large variations in hydrodynamic conditions and grain sizes that inevitably require filtering. Interpretation of the results of the modelling is a significant factor in determining its usefulness.

A single wave condition was modelled and produced reasonable-looking results. A complicated pattern of wave-induced currents was produced, including a series of vortices along the coast.

A storm with maximum offshore wave height of about 1.9m occurred near a neap tide. This produced a case with a relatively high waves and low tidal current, contrasting with the single spring tide. This was modelled 3 times with:

I Tidal flow only (no waves)
II A constant wave condition (using the same wave as for the single wave case)
III A time-varying wave condition, using measured waves as input.

At high and low tide the flow patterns were closer to the wave-only case than the spring tide case. At mid falling tide the strong estuary outflow plays a large role, but the flow patterns were still influenced by the wave-induced circulation. The modelled flows were not much affected by the presence of the waves at the offshore boundary points as the waves are not normally breaking. The effect of wave breaking was to increase the predicted flow velocities inshore. A visual inspection of the data is not sufficient to decide which model combination performs best. More objective methods of comparing model results are necessary and have been developed within the project.

The first steps towards compiling an objective set of model validation parameters have been taken by summarising available methods for comparing model performance. A number of these methods have been used with data from the spring tide case to assess PISCES' performance. The Brier Skill Score provides a measure of map-mean (or bias) phase and amplitude error and involves comparing to a baseline prediction (which can be a measure of the average climate). It therefore awards extra skill for modelling unusual or extreme events well. Its use is recommended although the choice of baseline model should be clearly stated. In the neap tide storm case the model results without waves could be used as the baseline prediction. Then the two cases with waves could be tested to see whether it is worth updating the wave input to the model every hour. In the spring tide case the model currents at the offshore boundary were used as the baseline prediction of currents at the measurement locations. The resulting Brier Skill Scores varied from 0.45 to 0.84 for current speed, showing that the model predicted the changes in the current well. The worst results occurred when transient spikes in the data were not reproduced accurately by the model.

It is recommended that longer time series of model results and measurements be used in future in the calculation of model performance statistics. Moreover statistics should be derived from the greatest umber of instruments possible.

10. REFERENCES

Ormondt, M van, The Teignmouth model, Validation and evaluation of Delft3D-MOR with COAST3D Pilot campaign data, WL|Delft Hydraulics report Z2394.20, February 2000.

Press WH, Teukolsky SA, Vetterling WT and Flannery BP, 1992. Numerical Recipes in Fortran, second edition. Cambridge University Press.

Ris RC, Holthuijsen LH and Booij, N, 1999. A third-generation wave model for coastal regions 2, verification. J Geophys Res 104(C4) 7667-7681.

Soulsby, RL, 1998. Coastal sediment transport: the COAST3D project. Proc 26th International Conference on Coastal Engineering, Copenhagen, June 1998, ASCE, pp. 2548–2558.

Soulsby, RL, 2000. Coastal study of three-dimensional sand transport processes and morphodynamics (project COAST3D). Proc EurOCEAN 2000, the European conference on marine science and ocean technology, Hamburg, 29 August – 2September 2000, pp 400–406.

Sutherland J and O'Donoghue T, 1997. CRF study of wave kinematics in front of coastal structures. Proc Coastal Dynamics '97. ASCE pp

Van Rijn LC, Ggrassmeijer BT and Ruessink BG, 2000. Measurement errors of instruments for velocity, wave height, sand concentration and bed level in field conditions. Dept. of Physical Geography, University of Utrecht, The Netherlands.

Whitehouse RJSW, Hearn S, Waters C, and Sutherland J, 2000. Data report on measurements by HR Wallingford at Teignmouth, UK (1998 – 1999). HR Wallingford Report TR105.

Zambreskey L, 1988. A verification study of the global WAM model, December 1987 – November 1988. GKSS Forschungzentrum Geesthacht GMBH Report GKSS 89/E/37.

Figures

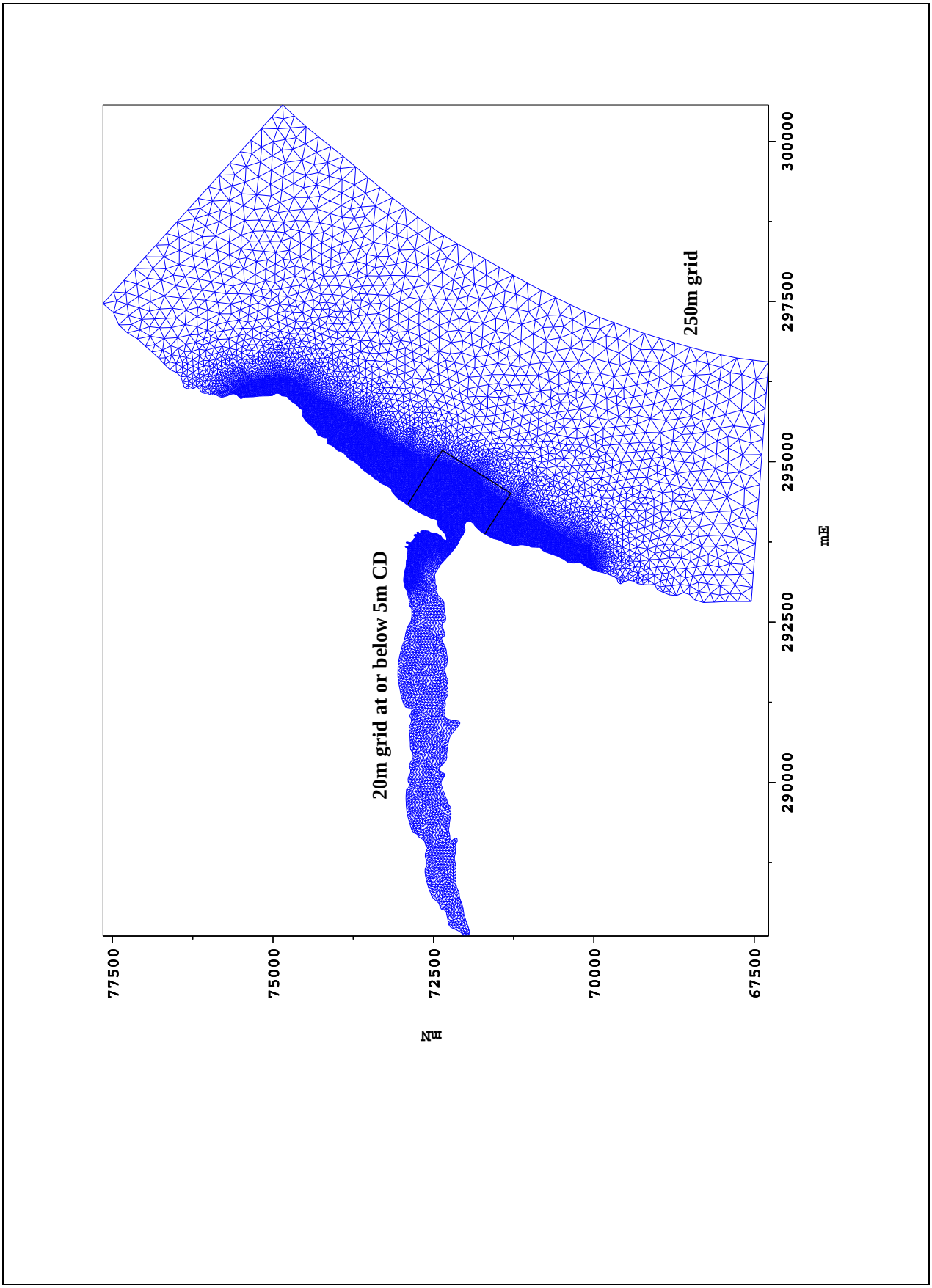

Figure 1 Flow model mesh

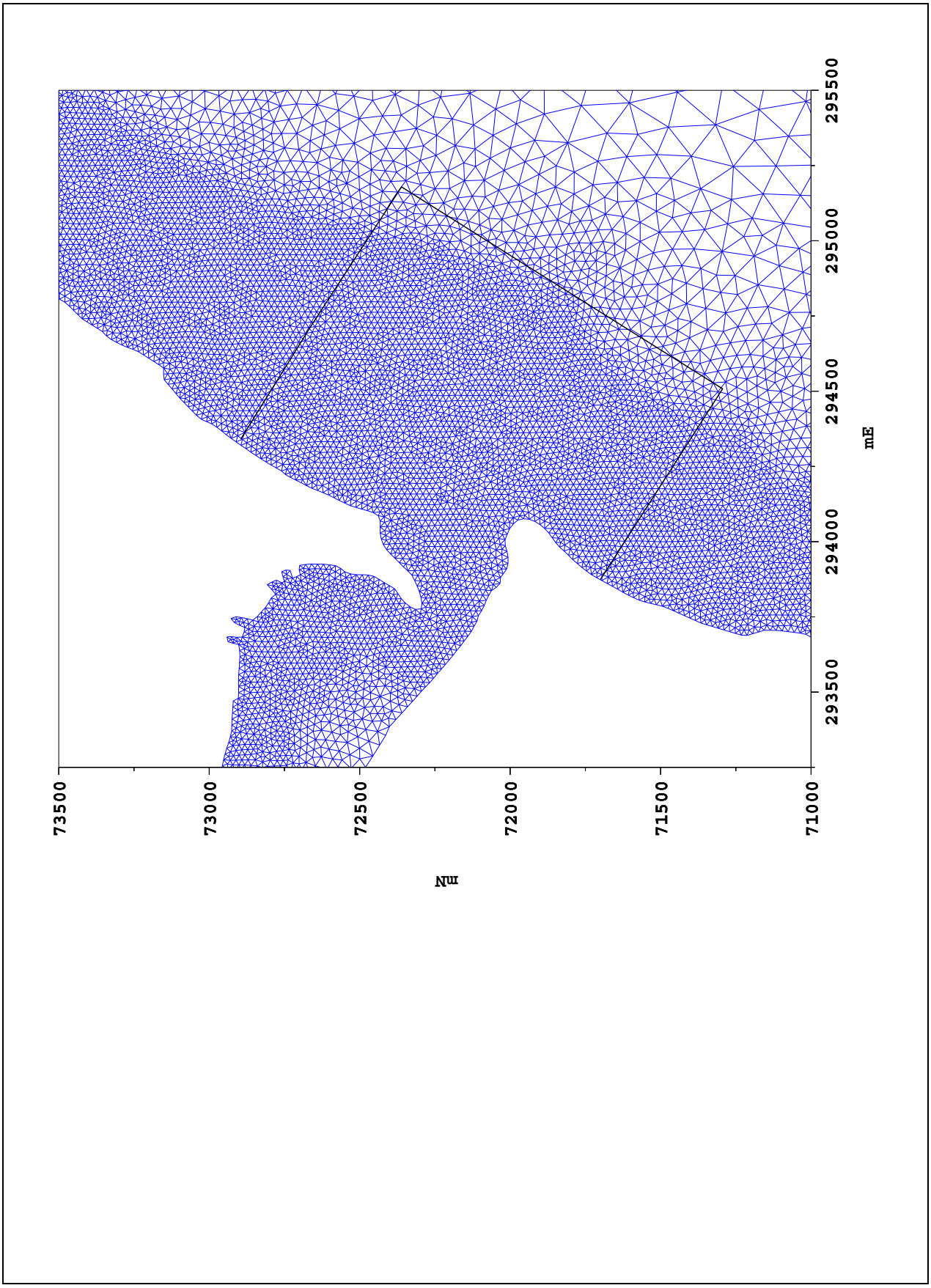

Figure 2 Flow model mesh, detail

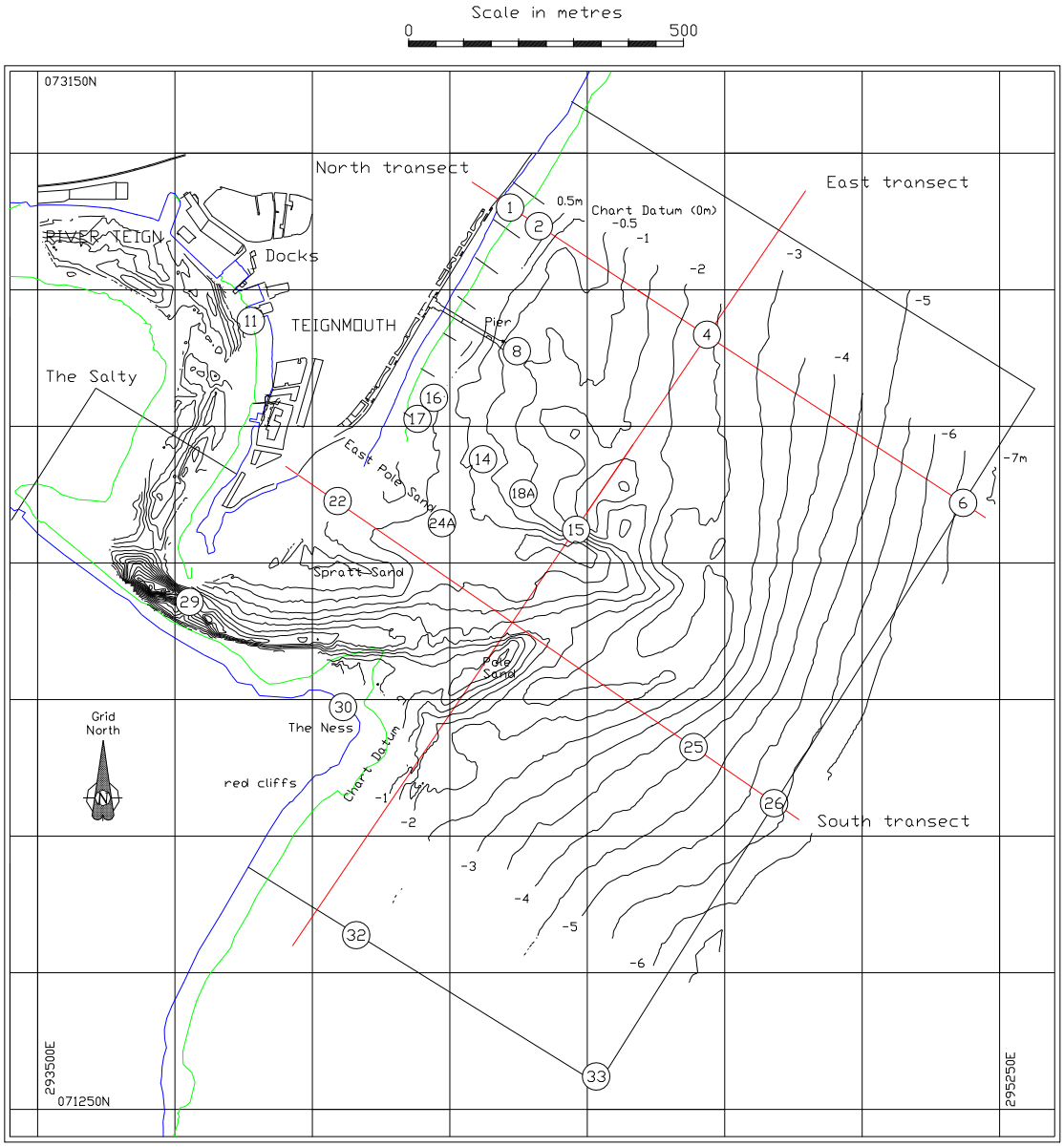

Figure 3 Pilot experiment instrument layout

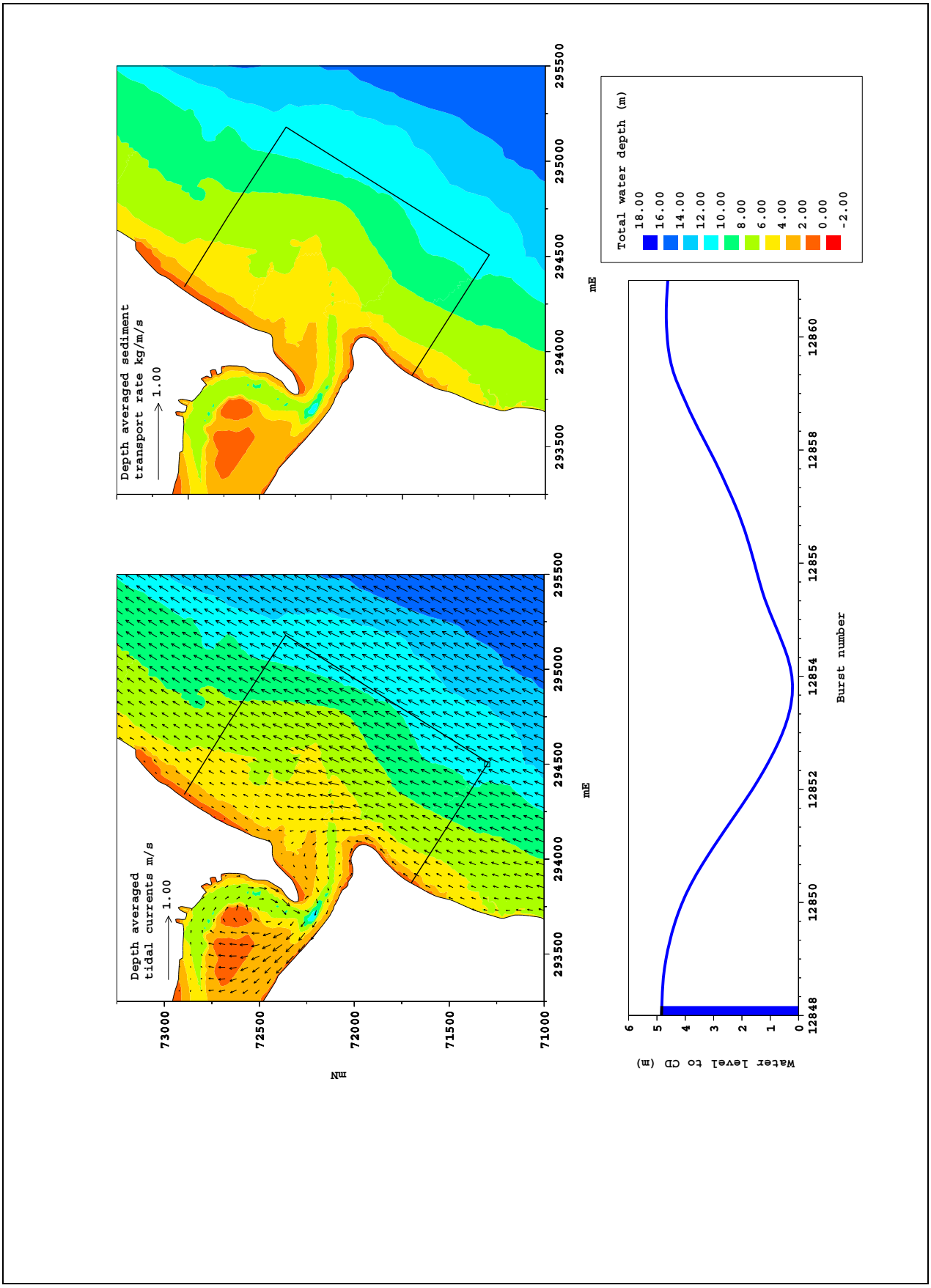

Figure 4 Spring tide-only current and sediment transport vectors at high tide

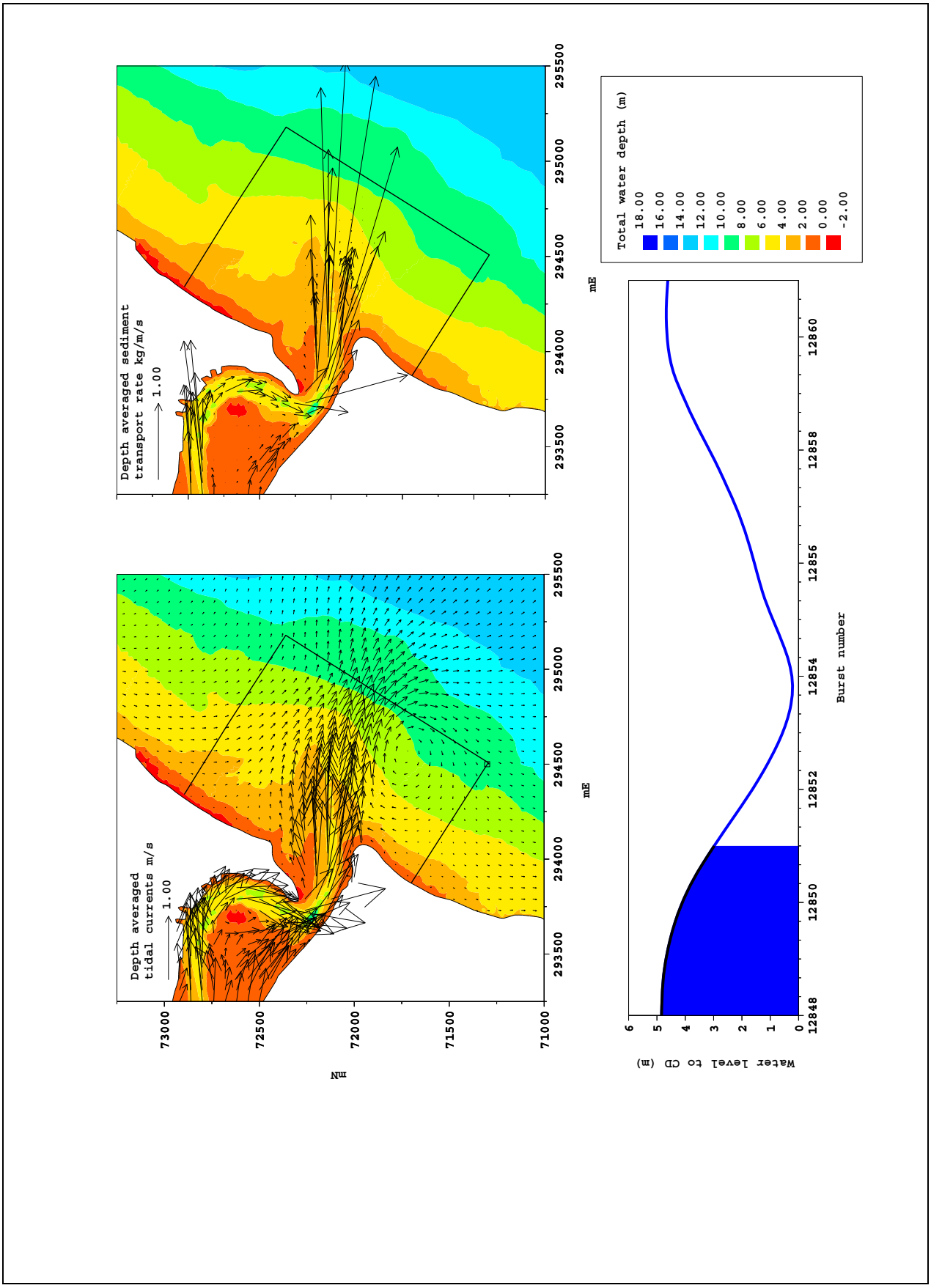

Figure 5 Spring tide only current and sediment transport vectors at mid (falling) tide

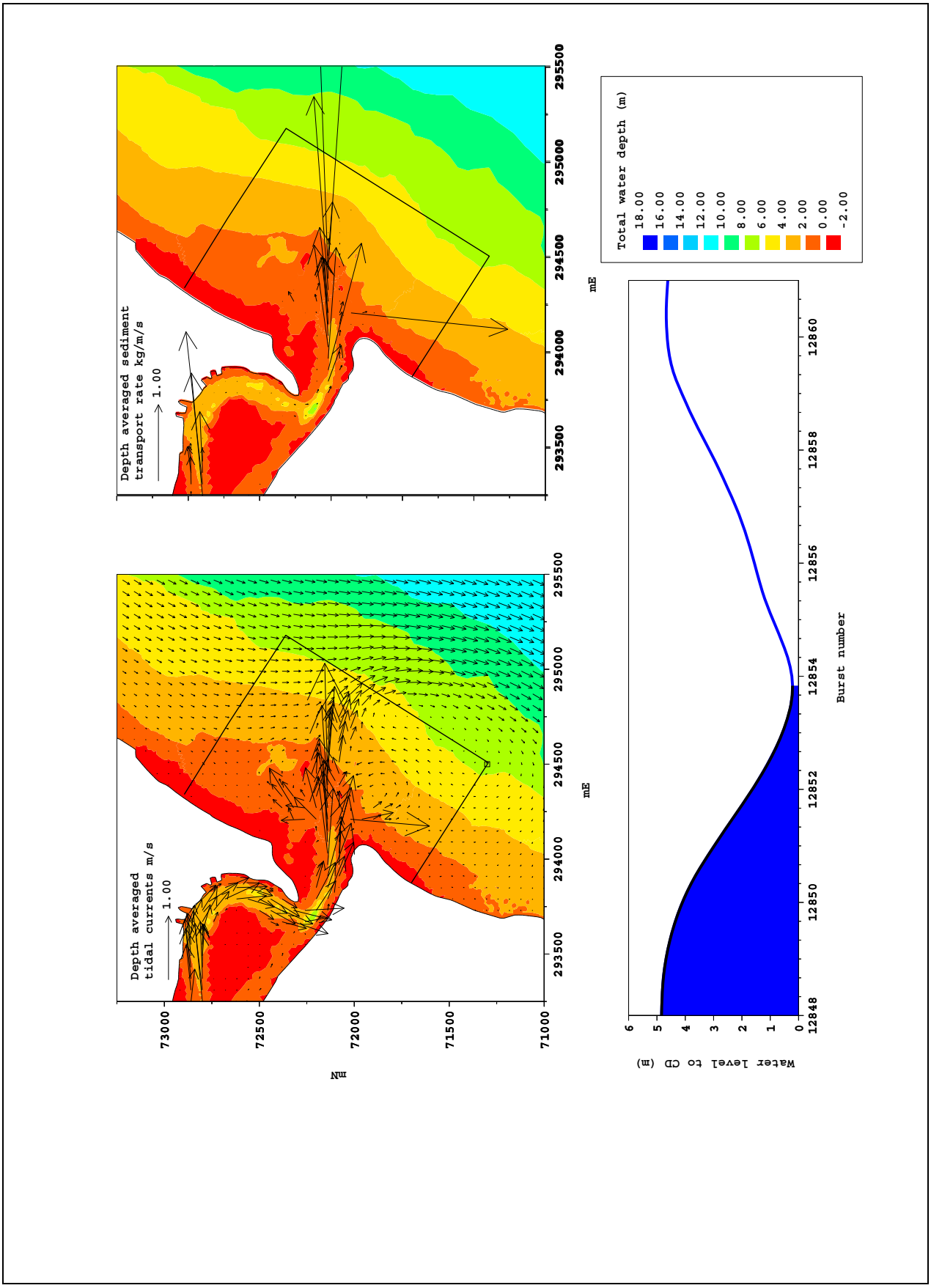

Figure 6 Spring tide only current and sediment transport vectors at low tide

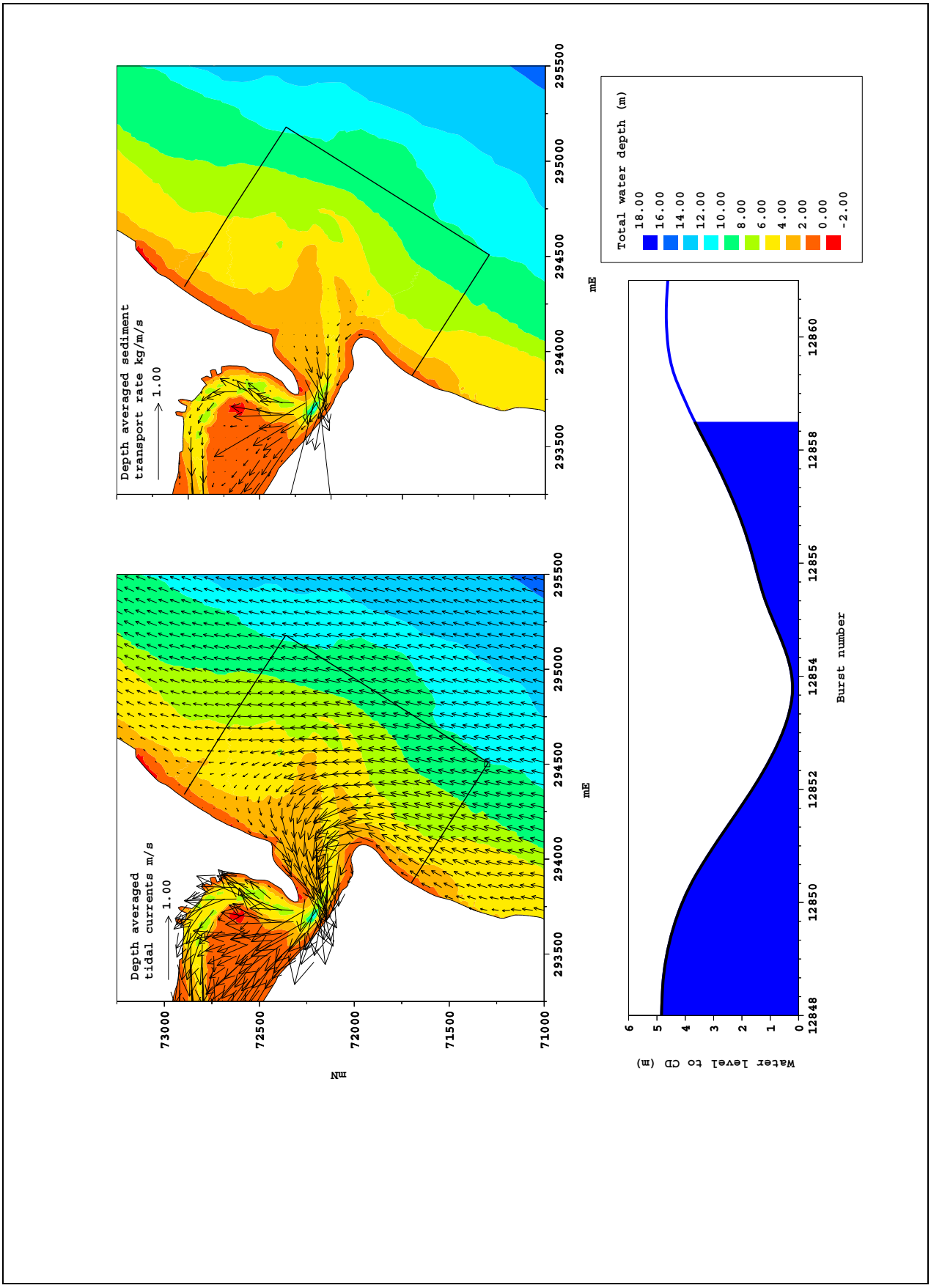

Figure 7 Spring tide only current and sediment transport vectors at mid (rising) tide

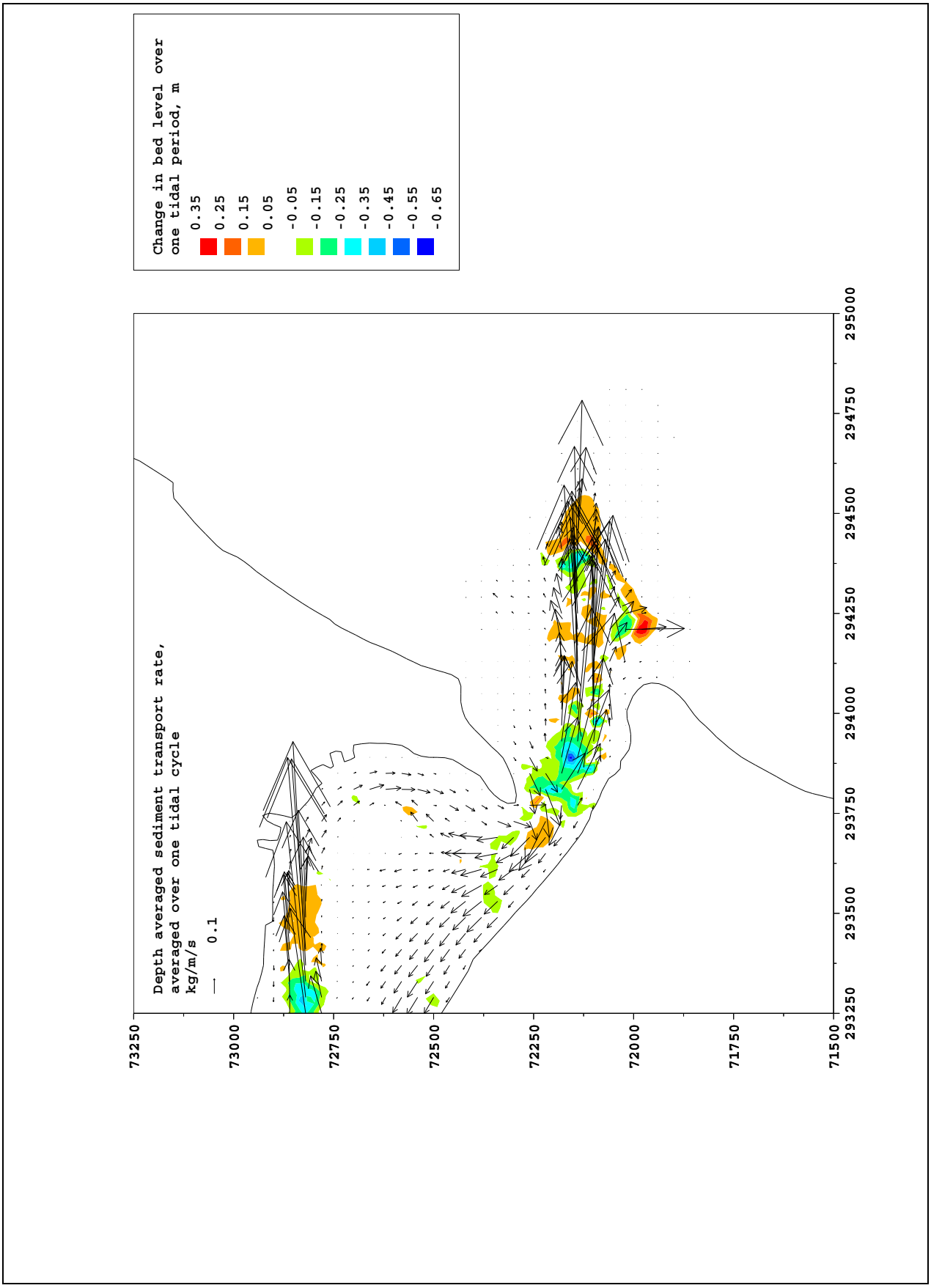

Figure 8 **Spring tide tidal residual sediment transport rate and changes in bed level over whole tide**

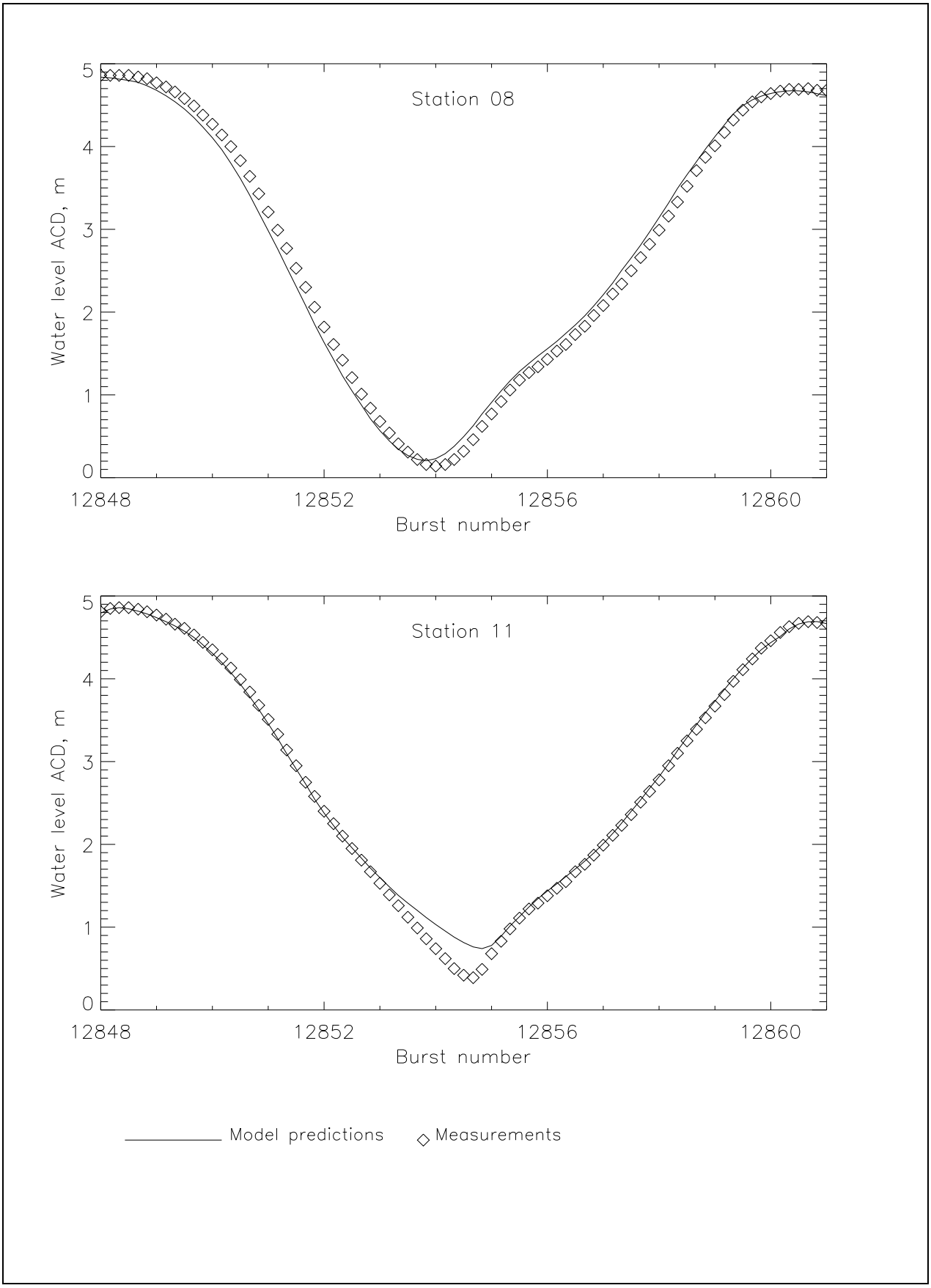

Figure 9 Spring tide only comparison of measured and predicted water levels at tide gauges

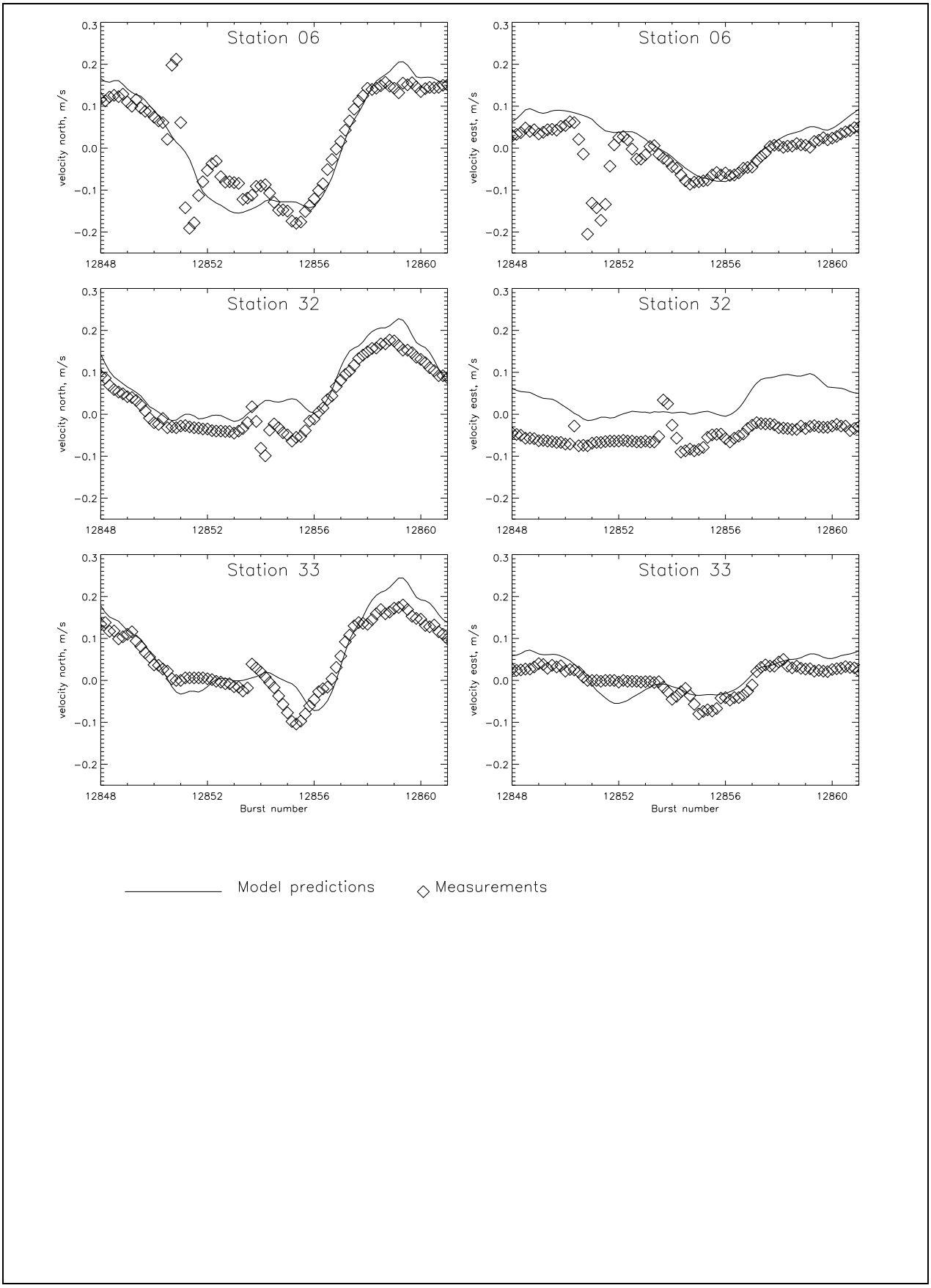

Figure 10 Spring tide only comparison of measured and predicted current velocities

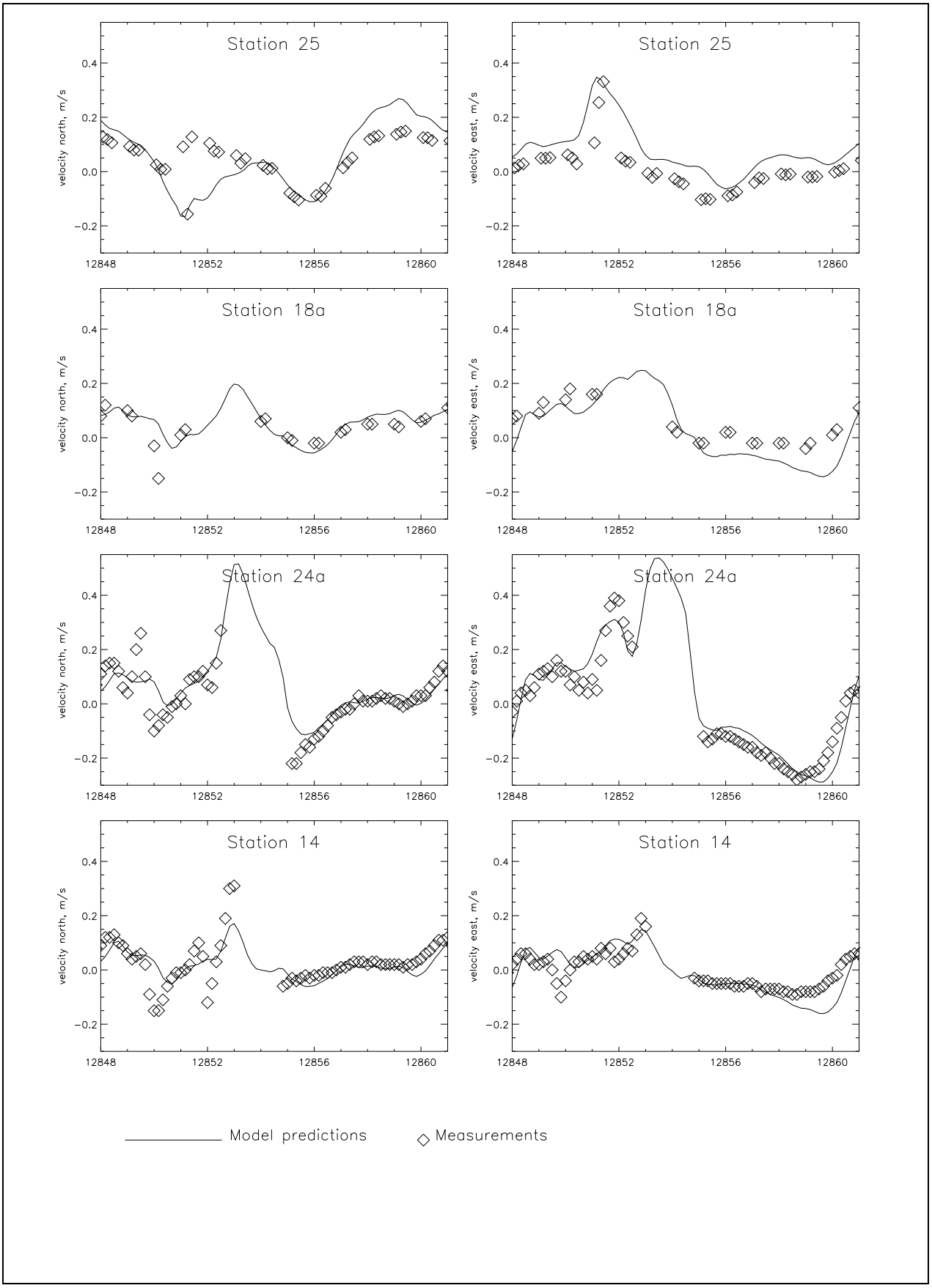

Figure 11 Spring tide only comparison of measured and predicted current velocities

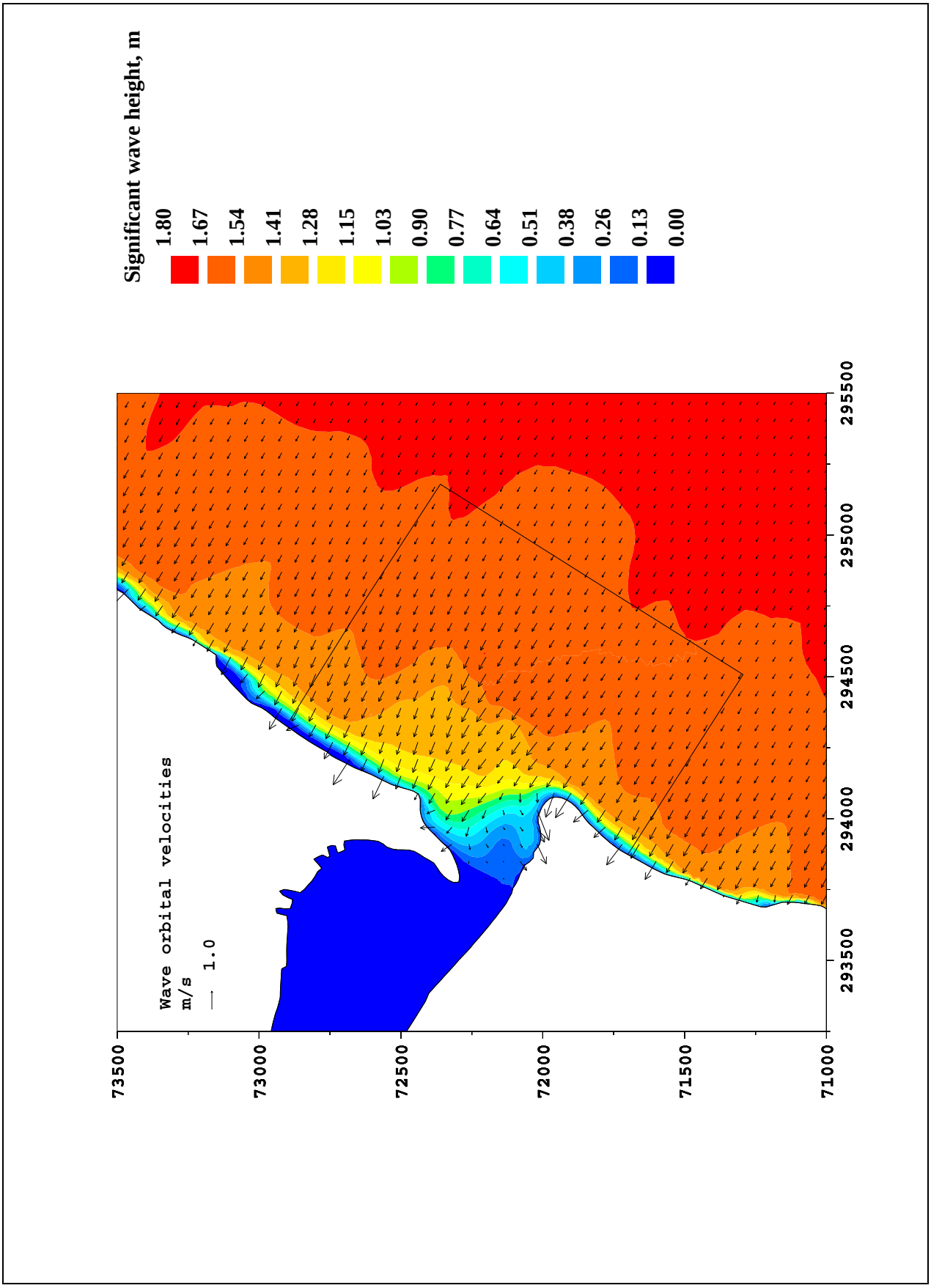

Figure 12 Wave only condition, wave heights and orbital velocities

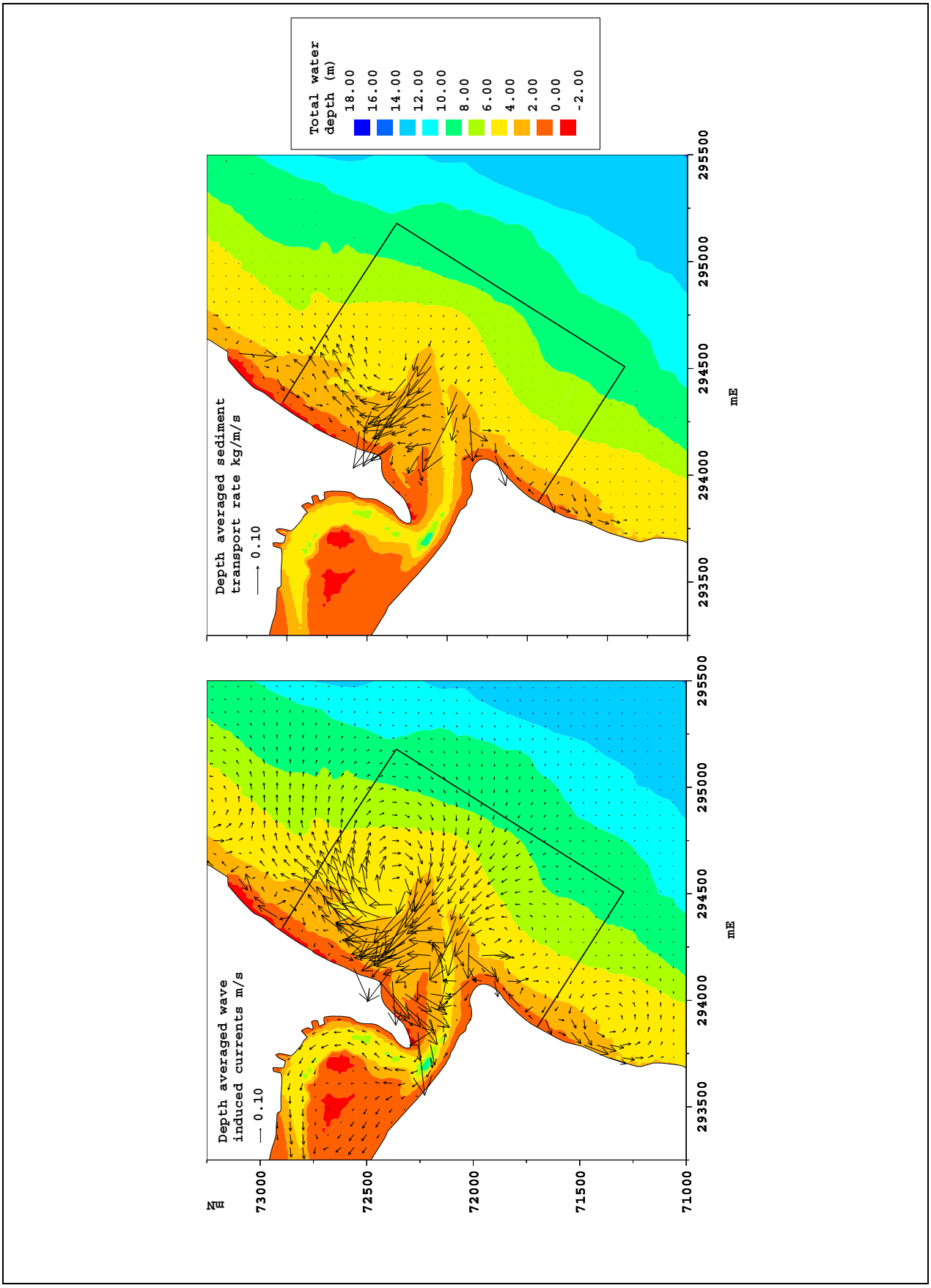

Figure 13 Wave only condition, current and sediment transport vectors

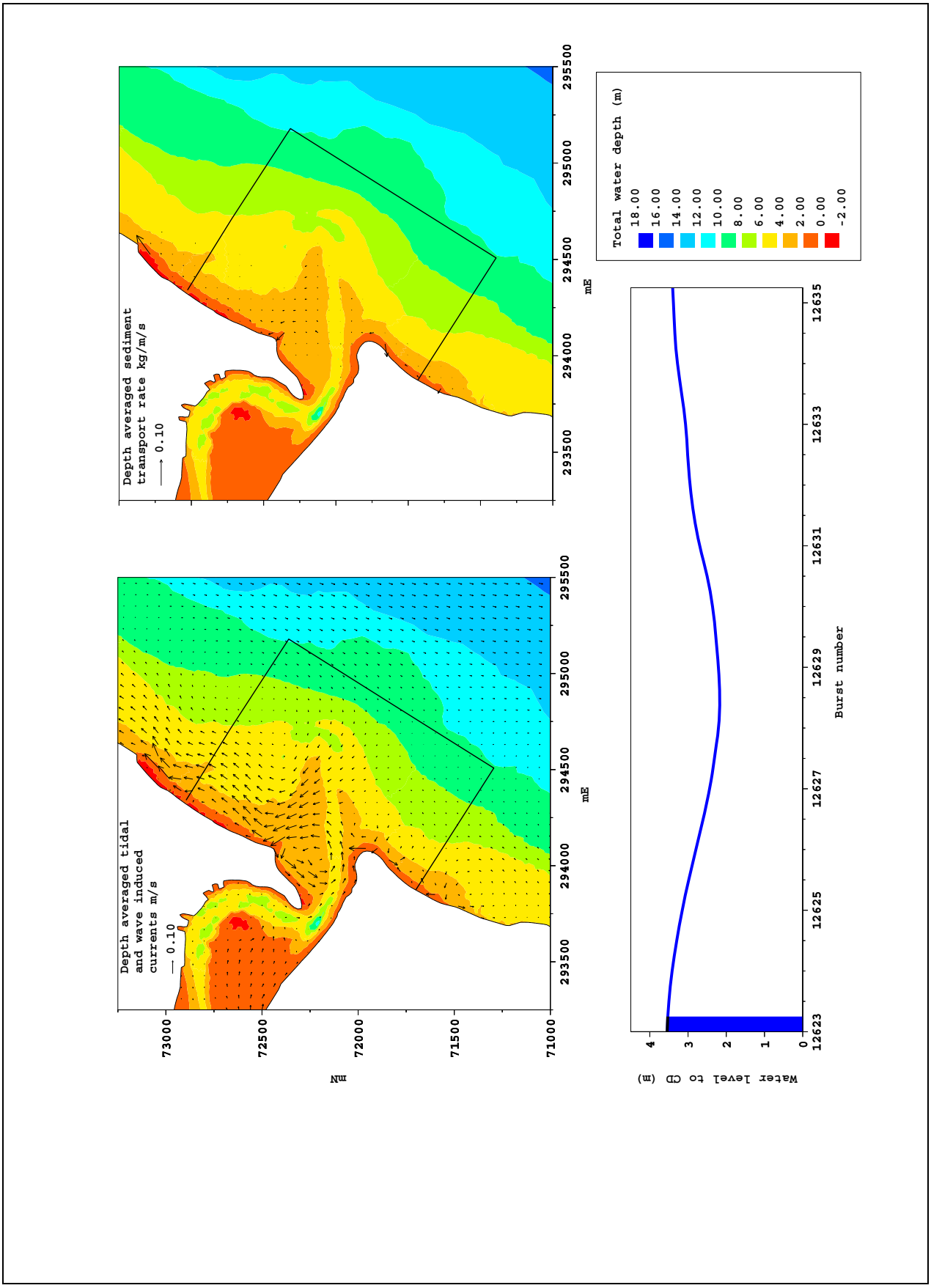

Figure 14 Near neap tide with changing waves: current and sediment transport vectors at high tide

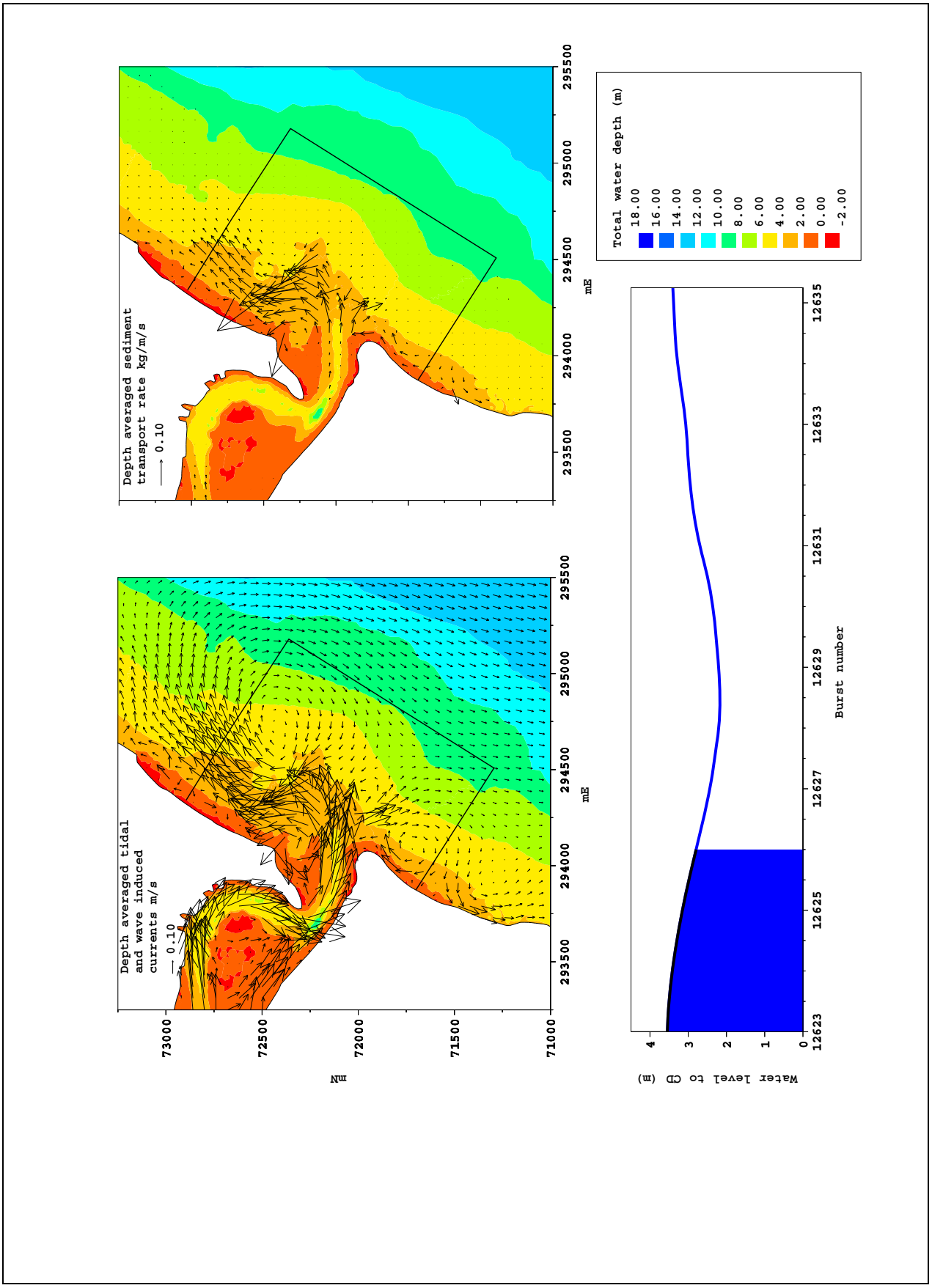

Figure 15 Near neap tide with changing waves: current and sediment transport vectors at mid (falling) tide

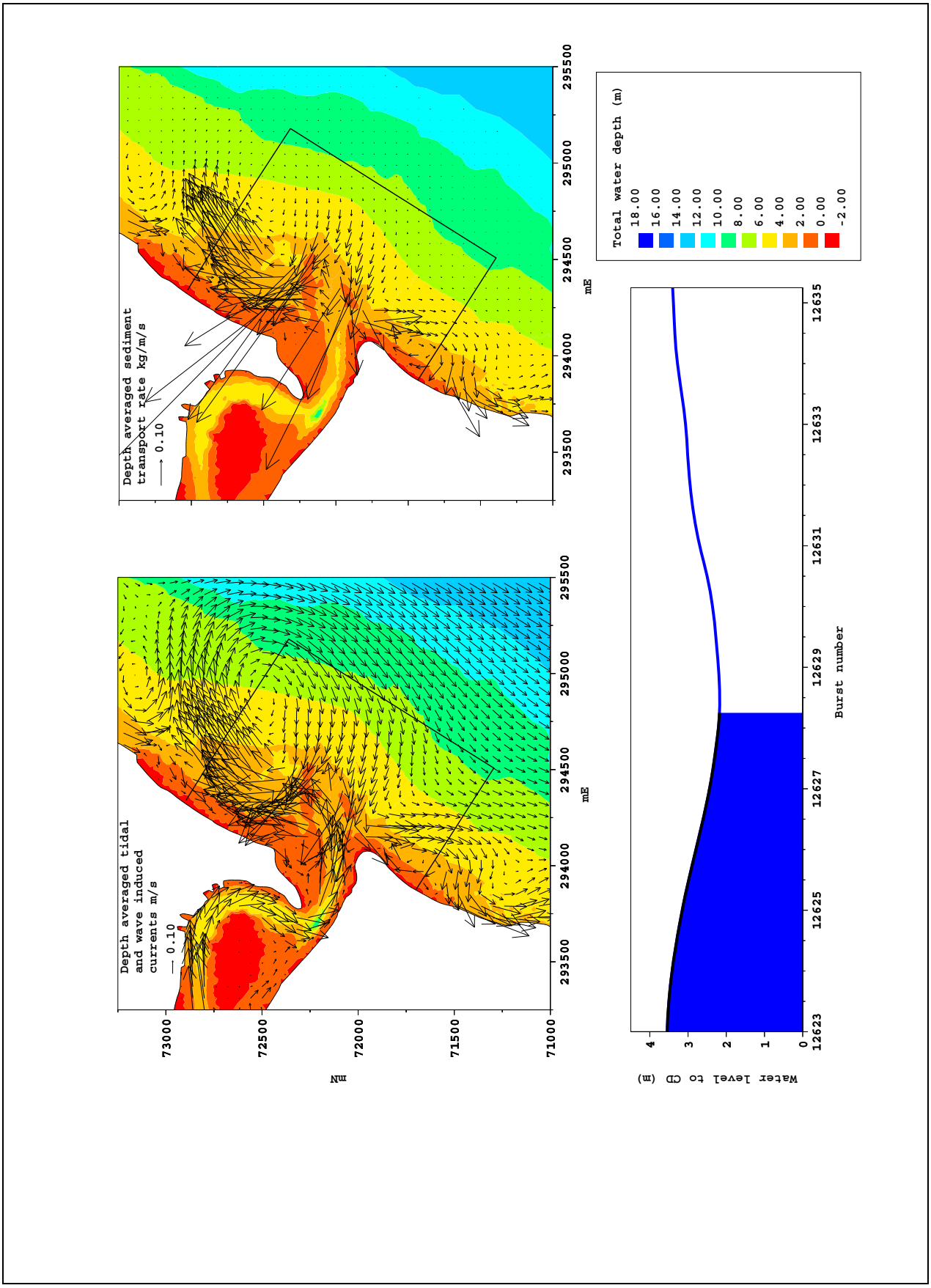

Figure 16 Near neap tide with changing waves: current and sediment transport vectors at low tide

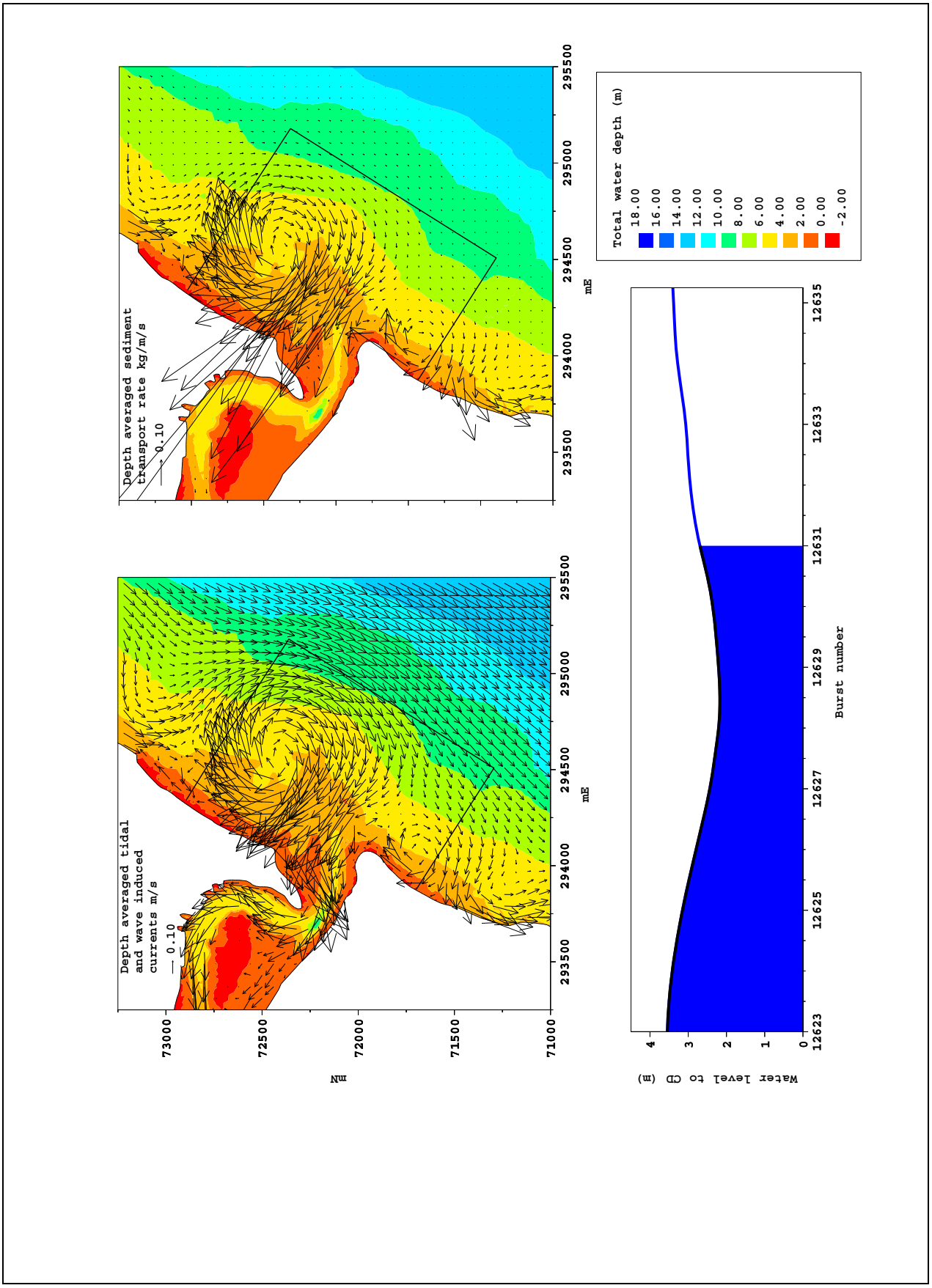

Figure 17 Near neap tide with changing waves: current and sediment transport vectors at mid (rising) tide

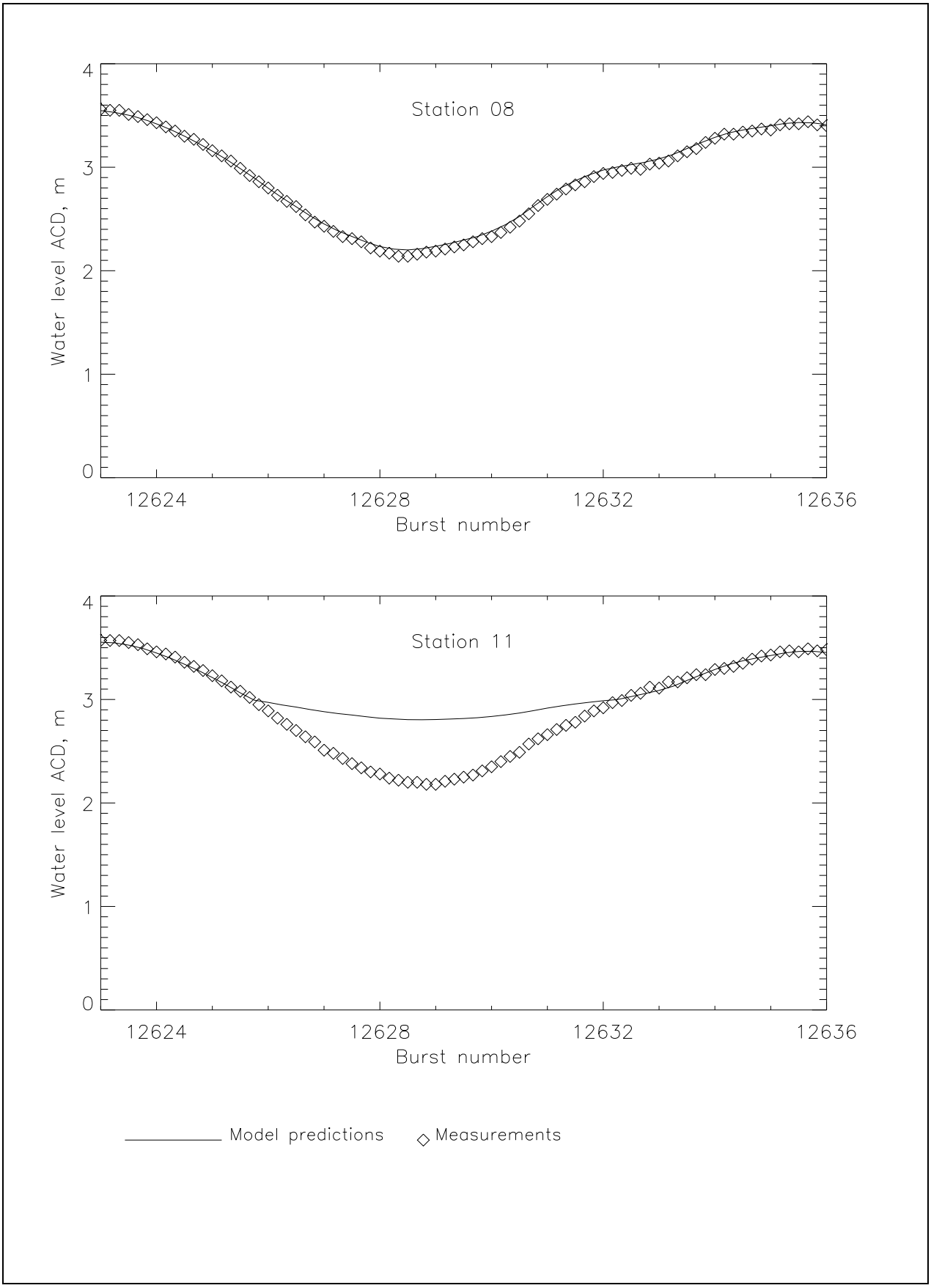

Figure 18 Near neap tide comparison of measured and predicted water levels at tide gauges

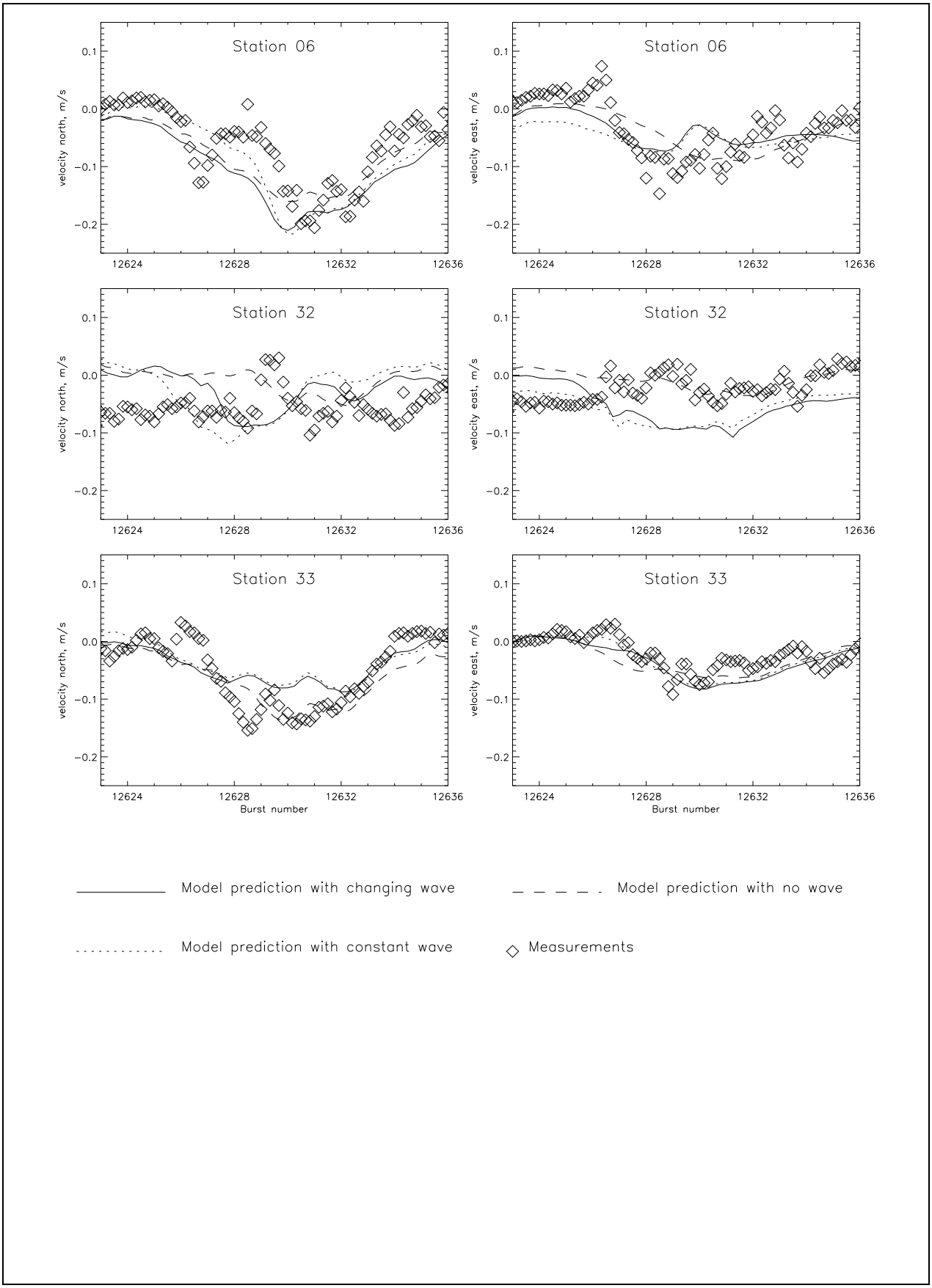

Figure 19 Near neap tide comparison of measured and predicted current velocities

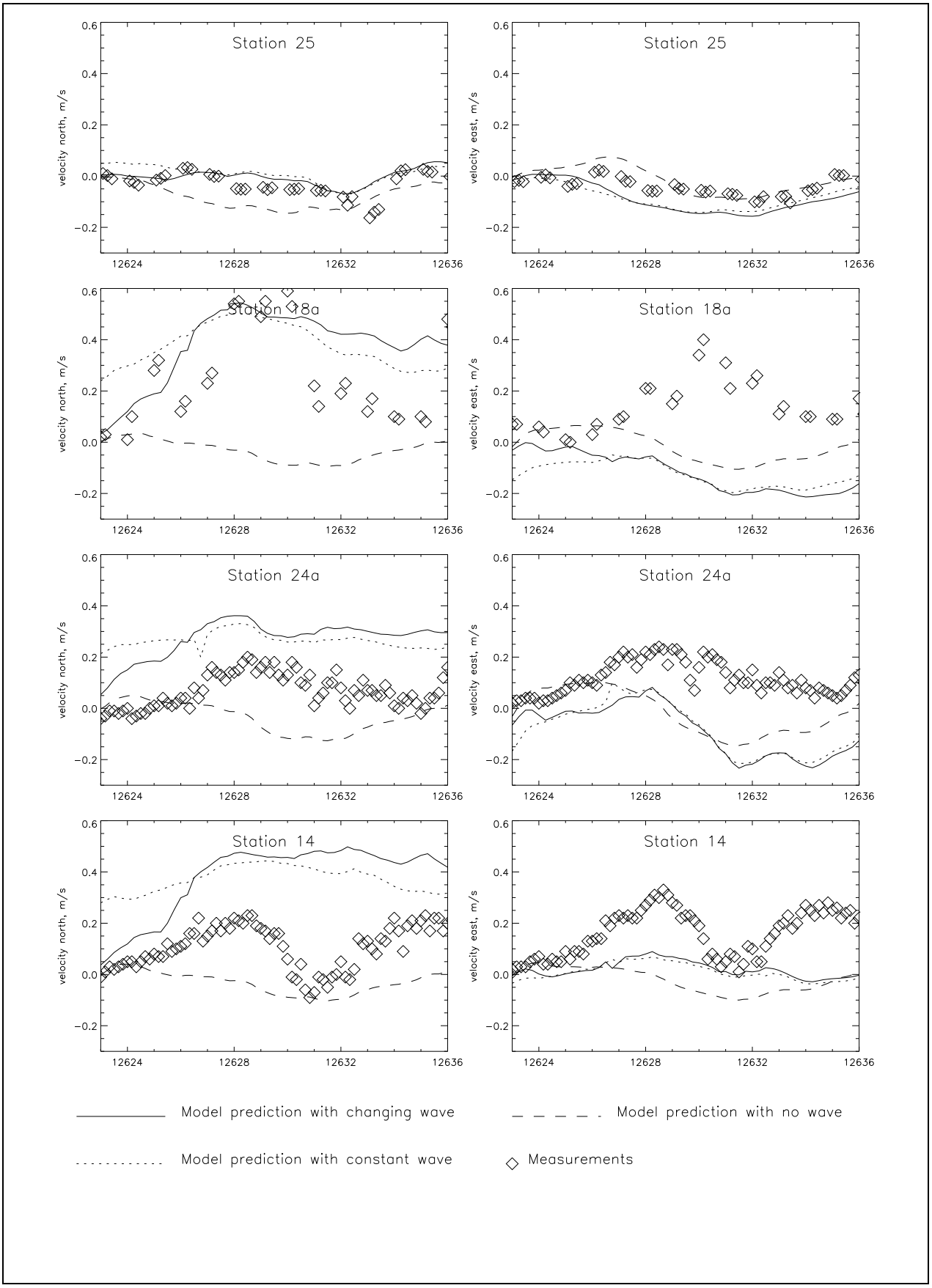

Figure 20 Near neap tide comparison of measured and predicted current velocities

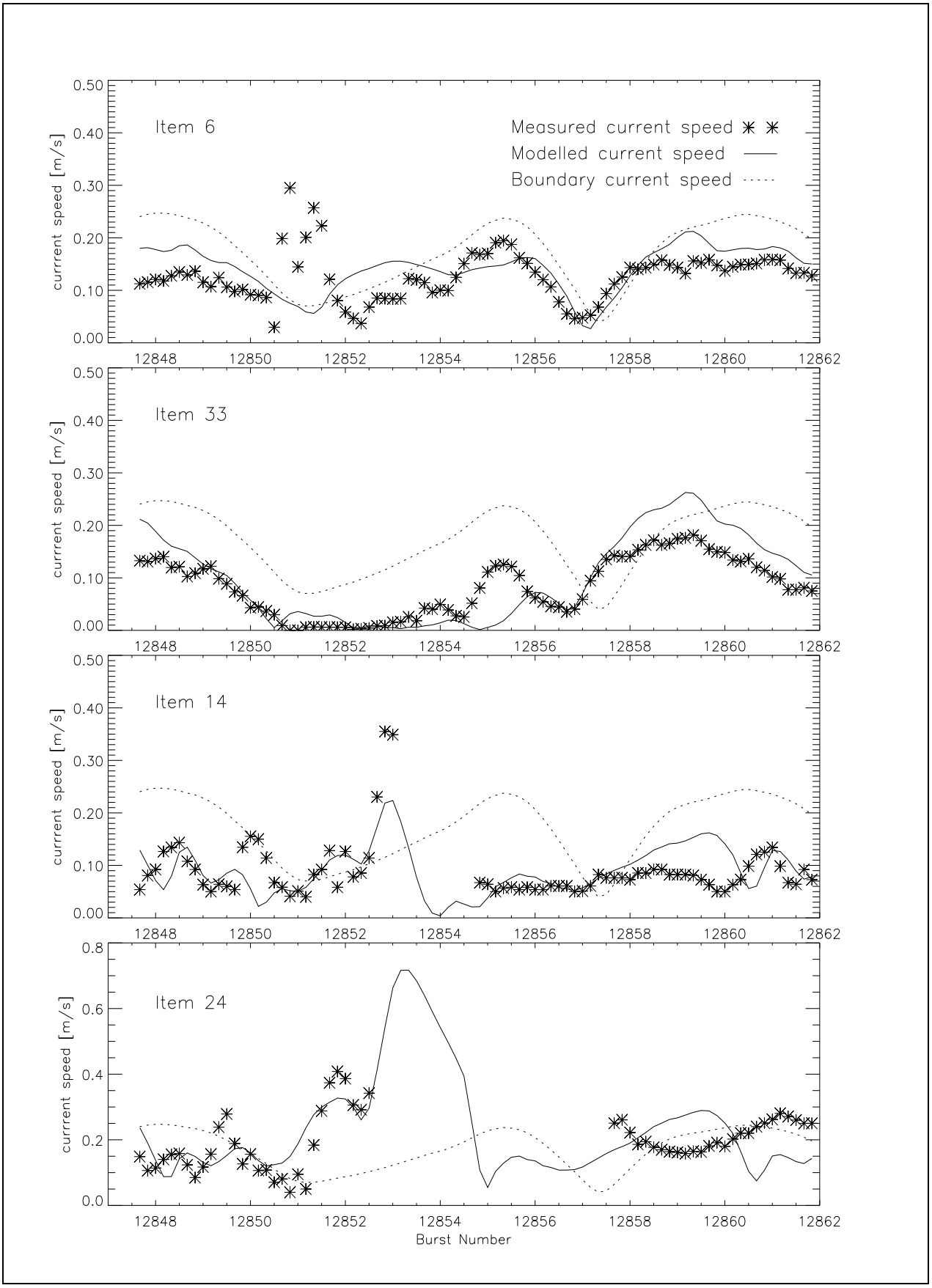

Figure 21 Spring tide measured and modelled current speeds with baseline prediction (boundary value)

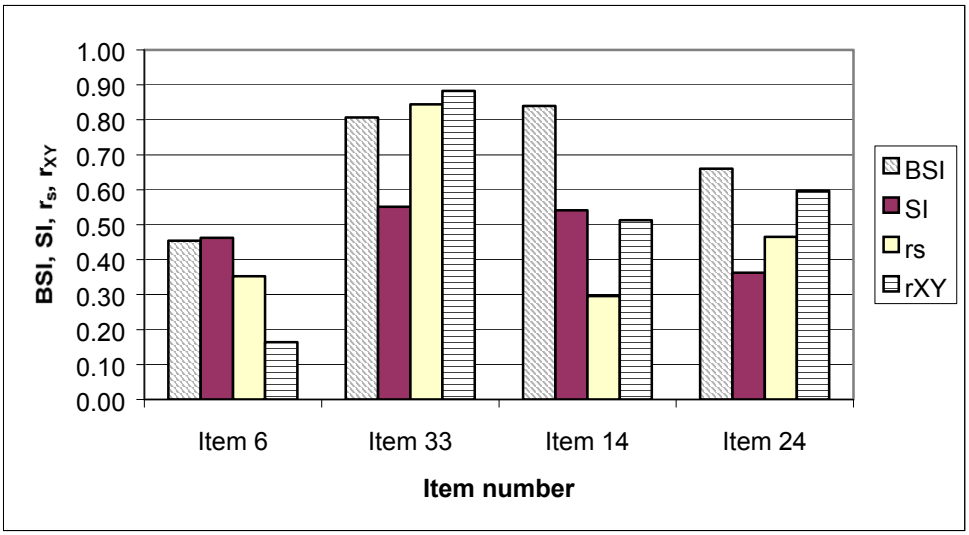

Figure 22 Brier Skill Score (BSS). Scatter Index, rank order (r_s) and linear (r_{xy}) correlations for current speed at items 6, 33, 14 and 24

Appendices

Appendix 1

The Telemac-2D Model

Appendix 1 The Telemac-2D Model

Description of Model and main areas of application
TELEMAC-2D is a sophisticated flow model, developed by LNH in Paris, for free surface flows. It solves the 2D depth-integrated shallow water equations which are used to model flows in rivers, estuaries and seas. TELEMAC uses finite element techniques so that very flexible unstructured triangular grids can be used. It has been developed under a quality assurance system including application to a standard set of validation tests.

The model can simulate depth integrated tidal flows in estuaries and seas including the presence of drying banks. It can also simulate flows in rivers including turbulence structures resulting from flow obstructions and transcritical flows. The model has been used with up to 30000 elements.

The advantage of using finite elements lies primarily in the possibility of using a very flexible grid. This is superior to using an orthogonal curvilinear grid as the user has more control over grid refinement resulting in accurate representations of complex coastlines. The applications of TELEMAC have included studies of ports, coastal management, floods in rivers, cooling water dispersion and infill of navigation channels.

Theoretical background and solution methods
TELEMAC solves the shallow water equations on an unstructured finite element grid (usually with triangular elements). The various variables (bed elevation, water depth, free surface level, u and v velocity components) are defined at the nodes (vertices of triangles) and linear variation of the water and bed elevation and of the velocity within the triangles is assumed.

When the model is used a timestep is chosen and the computation is advanced for the required number of timesteps. There is no particular limit on the timestep for a stable computation but it is best to ensure that the Courant number based on propagation speed is less than about 10. It is found that if the solution is nearly steady then few computational iterations are required at each step to achieve the required level of accuracy, which in TELEMAC is computed according to the actual divergence from the accurate solution. The computation at each timestep is split into two stages, an advective step and a propagation-diffusion step.

The advective step is computed using characteristics or streamwise upwind Petrov-Galerkin. The characteristic step makes it possible for the code to handle such problems as flow over a bump giving rise to locally supercritical flow and eddies shedding behind flow obstructions.

The finite element method used is based on a Galerkin variational formulation. The resulting equations for the nodal values at each timestep are solved using an iterative method based on pre-conditioned conjugate gradient (pcg) methods so that large problems are solved efficiently. Several pcg solvers are coded and a selection is available to the user. The complete matrix is not assembled, rather an element by element method is used so that most of the operations are carried out on the element matrices; this is computationally more efficient, both in speed of execution and in memory requirements. Rather than using Gauss quadrature exact analytical formulae are used for the computation of matrices. Symbolic software was used to draw up the formulae used. The software makes it possible to carry out a second iteration of the solution at each timestep in order to represent the nonlinear terms in a time centred way, otherwise these terms are treated explicitly.

Boundary conditions are applied at solid boundaries where a zero normal flow and slip or nonslip boundary conditions are applied. At open boundaries a selection of possibilities can be invoked depending on whether the flow is subcritical or supercritical, or whether a wave absorbing boundary using a Riemann invariant is needed. A water discharge along a boundary segment can also be applied and the software distributes the flow along the segment chosen. This facility is valuable when running models of river reaches and the discharge in a cross-section may be known rather than the velocity at each point in the cross-section.

The model can be run with a Cartesian grid for modelling rivers, estuaries and small areas of sea, with the ability to apply a uniform Coriolis parameter, or on a spherical grid for larger areas of sea in which case the Coriolis parameter is computed from the latitude at each node. The effect of a wind blowing on the water surface and causing a setup or wind induced current or of an atmospheric pressure variation causing an inverted barometer effect can be included, as can a k-epsilon model of turbulence if required.

The bed friction can be specified via a Chezy, Strickler or linear coefficient, or a Nikuradse roughness length. A variable friction coefficient over the model area is a possibility. Sidewall friction can also be included if required. Viscosity can be imposed as a given eddy viscosity value or a k-epsilon model can be used.

TELEMAC-2D includes the capability to simulate the transport of a tracer substance. The tracer is again computed using an advective step followed by a propagation/diffusion step. Tracer boundary conditions can be applied at model inflow boundaries. The tracer calculation has been used in order to simulate cooling water dispersion and mud transport. Sources of water and/or of tracer can be specified in terms of the discharge required and the x and y coordinates of the location.

Model Input
TELEMAC requires as input a finite element grid of triangles covering the area to be modelled. Bathymetric data from which the bed elevation at each node can be computed is also required. A file of keyword values is used to steer the computation (supplies bed roughness, timestep, duration of run etc).

The finite element grid may be generated using the MATISSE grid generator, which is part of the TELEMAC suite. The software STBTEL (part of the TELEMAC suite) is used to read the output file from the grid generation software. The bathymetry is input using a digitising tablet and the SINUSX software is used to capture the bathymetry data. The data is stored in a form to be read into the TELEMAC system and depths interpolated to the model nodes.

SINUSX is a powerful interactive graphical software that can be used to check and amend the input data. Bathymetric curves can be duplicated, deleted, smoothed, moved etc.

Model Output
The user can select a range of output parameters including u and v velocity, u and v discharge, water level, bed level, water depth, tracer concentration and Froude number. The TELEMAC output is contained in a single binary file which can be input to the graphics post-processor RUBENS. A listing file contains the input keywords and information on timestep reached, number of iterations to convergence etc. This file can be used to monitor the progress of a run.

Results from any part of the TELEMAC system are processed using the interactive graphics system RUBENS. This is a powerful and friendly environment where colour and black and white Figures can be produced interactively. By pointing and clicking time history plots, cross sections, vector plots and contour plots of any parameter at any position can be produced. Moreover parameters other than those input can be calculated in RUBENS and plotted.

11. REFERENCES

Hervouer, J.-M., 1991. TELEMAC, a fully vectorised finesse element software for shallow water equations. Computer Merhods and Water Resources, Robat, Morreco, 7-11 October. Also available as Electricite de Frnace report HE-43/91-27.

Hervouer, J.-M., 1994. The computation of free surface flours with TELEMAC: an example of evolution towards hydroinformatics. Journal of Hydraulic Research. Volume 32, extra issue pp45-64.

Appendix 2

The FDWAVE Model

Appendix 2 The FDWAVE Model

FDWAVE is a computational wave transformation model incorporating the combined effects of refraction and diffraction of waves using a time-independent finite-difference marching technique. This method has several potential advantages over alternative techniques. The inclusion of diffraction should give improved predictions of wave parameters compared with pure refraction methods in areas of irregular bathymetry where diffraction effects are strong. The method is also computationally quicker than most alternative refraction-diffraction methods, with the possibility of further increasing computational speed by the ability to use coarser grid sizes. Directional wave spectra, current refraction effects, and dissipation by bottom friction and wave breaking can be modelled. The model is designed for wave propagation in the open sea, rather than where structures are present. Wave directions are limited to a certain range either side of the forward grid direction, usually about 40° from this forward grid direction, but it depends on the grid being used.

The model is based upon a theoretical approach originally put forward by Battjes (Reference 1) and extended by Yoo and O'Connor (References 2 and 3). The HR FDWAVE model uses the same theoretical basis as Yoo and O'Connor but adopts a different numerical modelling approach. Yoo and O'Connor used a time-dependent formulation which can require a considerable number of time steps to reach a steady state. The present model is time-independent and gives the steady state solution directly. The theory and equations used in the model are described in detail in Reference 4.

The sea area under study is represented by a grid composed of rectangular or square elements. The positive y direction is chosen to be in the main propagation direction of the waves (roughly perpendicular to the coastline). The method of solution uses a row-by-row marching technique with a predictor and corrector calculation at each row. The input values of wave height period and direction are specified at each grid element on the offshore row. The finite-difference representation of the governing equations is then used to make a calculation of these parameters on the second row. This is the predictor step. Using these values, a more accurate estimate of the of the y-derivatives can be made, and the calculation of parameters on row two is repeated with these 'corrected' y-derivatives. This corrector step can, in principle, be repeated an indefinite number of times, but in most cases one calculation is found to be sufficient. The whole predictor-corrector process is then repeated for row three, and the process continues until the last row, furthest inshore, is reached. The method employed is explicit throughout.

References

1. Battjes J A. Refraction of water waves. Journal of Waterway and Harbour Division, ASCE, Vol 94. WW4, pp437-451, 1968.

2. Yoo D and O'Connor B A. Ray model for caustic gravity waves. Proc. 5th Conf. Of Asian and Pacific Division of IAHR, Seoul, Vol 3, pp 1-13, 1986.

3. Yoo D and O'Connor B A. Diffraction of waves in caustics. Journal of Waterway, Port, Coastal and Ocean Division, ACE, Vol 114, No 6, 1988.

4. Southgate H N and Goldberg D G. An efficient computational model for wave refraction and diffraction using finite differences. HR Report SR 213, June 1989.

Appendix 3

The SANDFLOW-2D Model

Appendix 3 The SANDFLOW-2D Model

Description of model and main areas of application
SANDFLOW-2D uses the flows calculated by the TELEMAC flow model to study the transport, deposition and erosion of non-cohesive (sandy) sediment and thereby identify areas of potential siltation and erosion.

Theoretical background and solution methods
The sediments under consideration here are very fine and fine sands (d_{50}~ 0.06 to 0.25 mm) which mainly move in suspension. The model can also be used to identify trends in the case of medium sand (d_{50}~ 0.25 to 0.5 mm).

The main factors controlling sand transport are:

- advection by currents
- settlement under gravity
- turbulent diffusion in all directions (but only the vertical component is of significance under most circumstances)
- exchange of sediment between the flow and the bed

The study of sand transport generally is very difficult but more so in the case of estuaries or coastal areas. This is because the water movements are continually changing, with the rise and fall of the tide, and there is usually a wide range of sediments on the bed and areas without mobile sediment, leading to unsaturated loads in the water.

Method
Although sand transport in estuaries is really an unsteady, 3D problem, it has been shown by HR Wallingford that it can be dealt with using a 2D, depth-averaged model provided special provision is made to account for the vertical profile effects of the sediment concentration. Under these circumstances the depth-averaged, suspended solids concentration c(x, y, t) satisfies the conservation of mass equation.

$$\frac{\partial}{\partial t}(dc) + \alpha\left[\frac{\partial}{\partial x}(duc) + \frac{\partial}{\partial y}(dvc)\right] = \frac{\partial}{\partial s}\left(dD_s \frac{\partial c}{\partial s}\right) + \frac{\partial}{\partial n}\left(dD_n \frac{\partial c}{\partial n}\right) + S \qquad (1)$$

where

(u,v)	=	depth-averaged components of velocity (m/s)
D_s	=	longitudinal (shear flow) dispersion coefficient (m5/s)
D_n	=	lateral (turbulent) diffusivity (m5/s)
(x,y)	=	Cartesian co-ordinates in horizontal plane (m)
(s,n)	=	natural co-ordinates (parallel with and normal to mean flow) (m)
t	=	time (sec)
d	=	water depth (m)
S	=	erosion from or deposition on the bed (kg/m5/s)
α	=	advection factor to recover the true sediment flux from the product of depth-averaged quantities

Advection factor (a)
This is introduced to compensate for the omission of the vertical profile in the sediment flux terms.

$$\alpha = T/qcd \qquad (2)$$

where

T = $\int_o^d 1$ q'c'dz is the sand transport (kg/m width/s)

q = the depth-averaged water speed $(u5 + v5)^{1/2}$
and q',c' are the full three-dimensional velocity and concentration variables.

Since the highest concentrations occur near the bed it follows that $\alpha \# 1$. Typical values of α can be obtained by evaluating equation (2) for sand transport profile observations or from the integration of theoretical solutions for suspended solids profiles. However, in practice, it is usually acceptable to take $\alpha = 1$ on the grounds that the external and internal sources of mobile sediment are not well enough known to justify a more precise formulation.

Bed exchange relations
The simplest formulation of the bed exchange relation is

$$S = ß_s \omega_s (c_s - c) \qquad (3)$$

where
c_s is the depth-averaged concentration when the flow is saturated with sediment (kg/m^3)
ω_s is the representative settling velocity (m/s)
$ß_s$ is a profile factor to compensate for integrating out the vertical profile of suspended sediment ie to correct for higher sediment concentrations near the bed.

Deposition or erosion takes place depending on whether the instantaneous sediment load (c) exceeds or is less than the saturated value (c_s). Pick up of sediment from the bed is prevented if there is no sediment available on the bed. A shortage of material on the bed is reflected in a low concentration of suspended solids being advected away by the flow.

Typical values of $ß_s$ could be obtained from actual observations of sediment profiles or from theoretical considerations. However, HR Wallingford have derived an analytical expression for this so that bed exchanges are performed automatically. This involves simplifying the vertical diffusivity relation and a profile mixing factor is introduced to enable the user to increase or decrease the effective mixing during calibration of the model.

Sediment transport relations
The evaluation of bed exchanges requires a depth-averaged sediment concentration (c_s). Sandflow-2D obtains this from a sediment transport relation specified by the user. Three sand transport relations are supplied in the package (Ackers-White, van Rijn and a simple power law) and since the source code is provided other relationships can be added by the user if preferred.

The choice of sand transport relation needs care. It should be borne in mind that most relationships found in the literature are based on river or channel data where sediments are more narrowly graded than in estuaries. Also there is normally a small proportion of cohesive material in estuary sediments and this can alter the transport properties. If possible, sand fluxes should be measured at the study site, and if such data is available it may be best to use it to obtain the best-fit power law relation for the site.

Diffusion
The dispersion (D_s) and diffusion (D_n) coefficients are not well defined. When viewed in close enough detail the whole motion appears advective; but when viewed on a coarser grid the smallest motions appear diffusive. Thus selection of the appropriate diffusion or dispersion coefficients depends on the grid size of the model - one model will treat as advection what a coarser grid model will treat as diffusion or dispersion.

Fortunately, the solutions to the equation are not normally sensitive to D_s and D_n. As a first approximation, $D_n = Bdu$, where d and u are representative depths and velocities. It has been found that B is usually in the range 0.01 (for fairly uniform depths and smooth beds) to 0.1 (for irregular geometry and/or rougher beds).

D_s is automatically calculated by the program for each model cell depending on the local depth and velocity to give more diffusion in the direction of flow. The overall scale of D_s can be changed using the relative dispersion parameter (in keyword DIFFUSION). This normally has the value unity but it can be adjusted upwards or downwards during calibration to get agreement between the model results and any dispersion observations which may be available.

Numerical Model
A simple, explicit, upstream finite difference technique is used to solve the advection - diffusion equation. Flux corrections are not considered to be necessary because the background concentrations of suspended sand are normally fairly uniform throughout the model in contrast to POLLFLOW-2D applications which have one or two point sources and correspondingly steeper concentration gradients.

The use of an explicit method introduces a stability constraint on the computing timestep (Δt).
$\Delta t < \Delta s/$(maximum flow velocity)
where Δs is the grid size (m):

Generally, this does not pose any problems in practice because the allowable Δt is usually much larger than the TELEMAC timestep. Under these circumstances an explicit method is preferred because it enables the user to understand the code more easily and to modify the treatment of the physics of the processes being simulated.

The treatment of the dispersion (D_s) and diffusion (D_n) terms introduces another stability constraint.
$\Delta t < \Delta s5/4$ Dmax
where Dmax is the maximum of D_s and D_n.

This constraint is normally weaker than the advective stability limit but a high value of diffusivity can lead to an instability. In the event of problems the possible violation of both limits should be checked.

Inputs
SANDFLOW-2D requires as input the elevation and flow results from a TELEMAC run, together with information describing the initial distribution of sand on the bed. A boundary data file is also required to specify sediment concentrations at the model edges with respect to time. Other parameters required include the typical size of sand and its basic properties such as settling velocity and threshold stress for initiation of motion.

Data is input to SANDFLOW-2D using ASCII data and steering files and unformatted direct access results files from TELEMAC.

Time to setup/calibrate/run/amend model
The time taken to setup and run a SANDFLOW-2D model obviously depends upon the extent of the modelled area, availability of data, test conditions specified and the computer used. However, as a guide the following estimates are for a typical 25000 cell model using a SUN IPC sparcstation or 486 Personal Computer.

Setup boundary data: one day
Preparation of SANDFLOW-2D steering file: thirty minutes
Run model for one tide: one to three hours
Note that the SANDFLOW-2D results should be carefully interpreted before planning further runs.
Amend steering file: five minutes
Amend boundary conditions: 2 hours

It should be remembered that these times are additional to that required to run TELEMAC.

Outputs

SANDFLOW-2D calculates concentrations of suspended sediment and distributions of erosion and deposition are stored at user selected intervals during the run. SANDFLOW-2D calculates suspended sediment concentration, erosion and deposition throughout the model area for each timestep through the tide.

Each run of the SANDFLOW-2D model generates three output files. Two of these files contain the suspended concentrations and bed deposits. The third output file, the List File contains run information. Contour plots of suspended concentrations and/or bed deposits at user selected times and concentration-time and deposit-time plots at selected locations can be produced.

Appendix 4

Waves and tides during the pilot experiment

Appendix 4 Waves and tides during the pilot experiment

The variation in spectral significant wave height at locations 4, 6, 26, 33 and 32 around the edge of the experimental area throughout the Pilot Experiment is shown in Figure 1. There is a moderately severe storm at the start of the experiment followed by very low wave conditions during the rest of the time. Time is measured in burst numbers – the number of hours after 00:00 on 1 October 1997. Each burst is one hour.

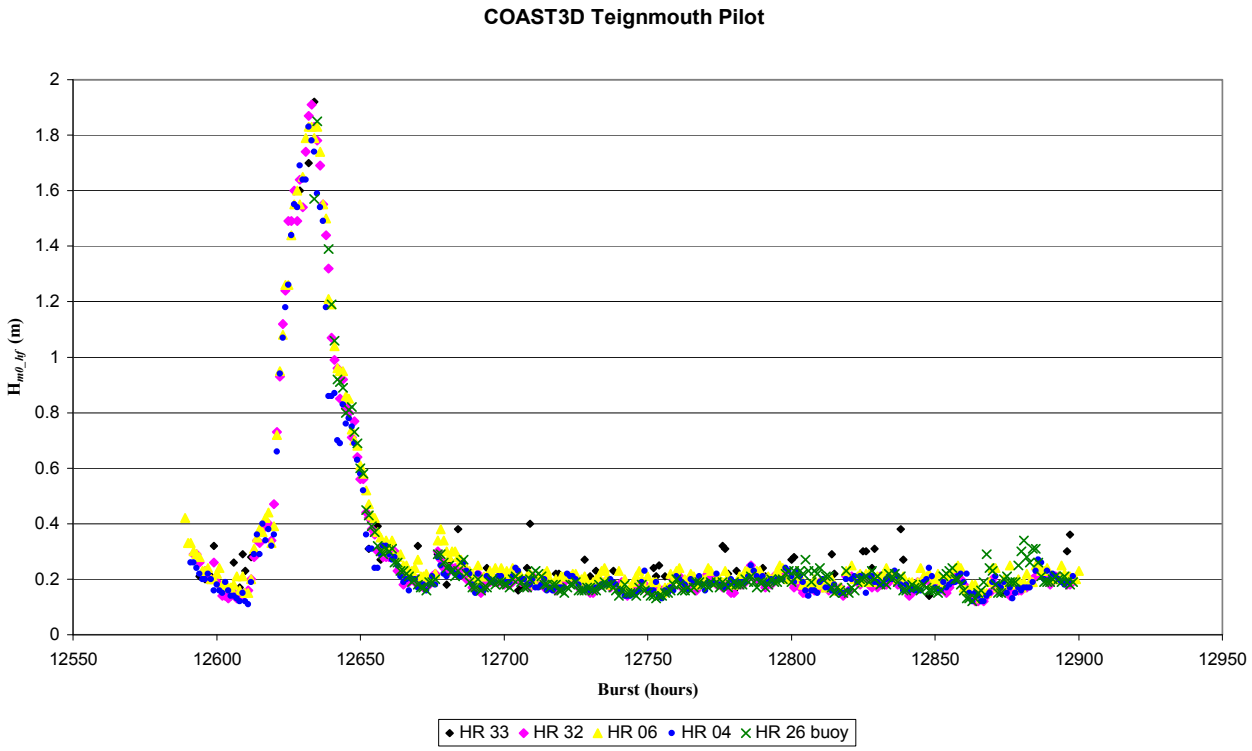

Figure 1. Spectral significant wave height through the Pilot experiment

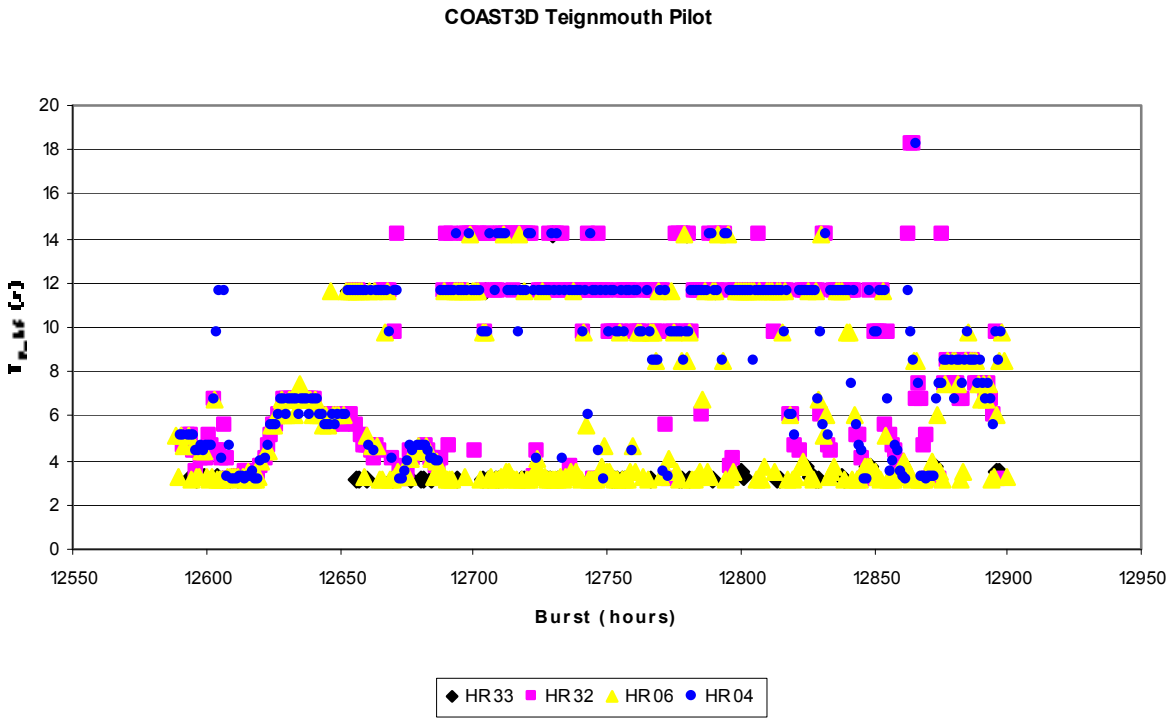

Figure 2. Spectral peak period through the Pilot experiment

Figure 2 shows the measured spectral peak periods through the Pilot Experiment. During the storm the periods are all very similar and build up to between 6 and 7 seconds during the peak of the storm. Following the storm, when there are low waves there is a much wider scatter in the results. The wave heights during this period are typically less than 0.2m, some of which is locally generated and some of which is swell. The different instruments pick out different parts of the spectrum, indicating that peak period is not a stable parameter for very low waves.

The tide gauges at locations 8 and 11 make the only really accurate measurements of water level. These are shown in Figure 3. At different stages of the tide (especially around low water) there are noticeable differences in water level between the tide gauge in the estuary (11) and the open sea (8) due to the throttling effect of the estuary mouth. Admiralty Chart Datum (Teignmouth Approaches) is 2.65m below Ordnance Datum Newlyn (ODN).

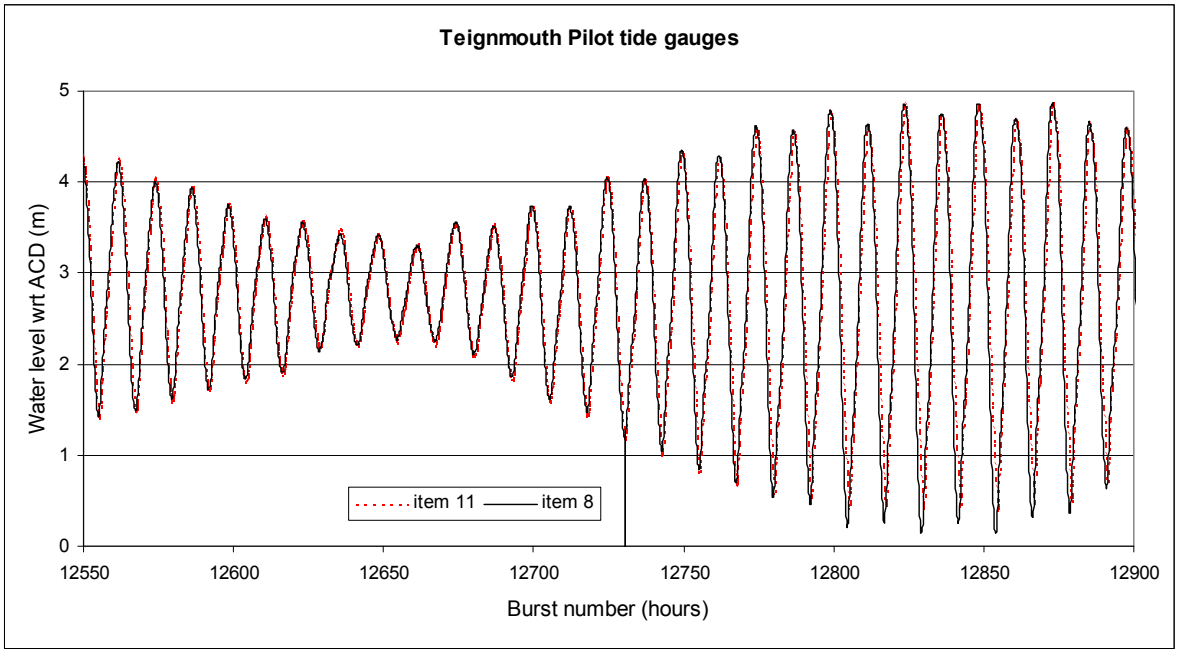

Figure 3. Water levels with respect to Admiralty Chart Datum (Teignmouth Approaches)

The water levels during the single spring tide test case are shown in Figure 4. The wave heights are so low that this case was modelled using flow models alone. The dashed lines mark the start and end of the modelled tide.

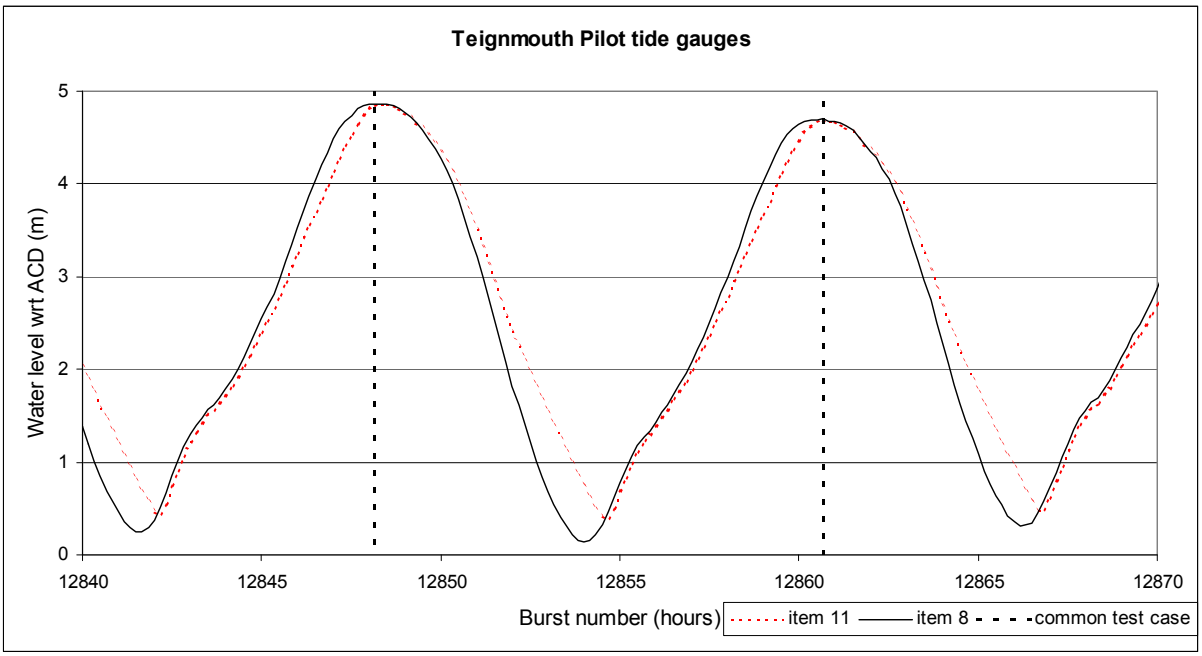

Figure 4. Water levels at tide gauges during single spring tide common test case.

During the near-neap tide with storm test case the wave heights and water levels both varied during the modelled tide. The wave heights around the experimental area boundary (left hand axis) and water levels at the Pier tide gauge (right hand axis) are plotted against burst number in Figure 5. The dashed line shows the start and end of the test case.

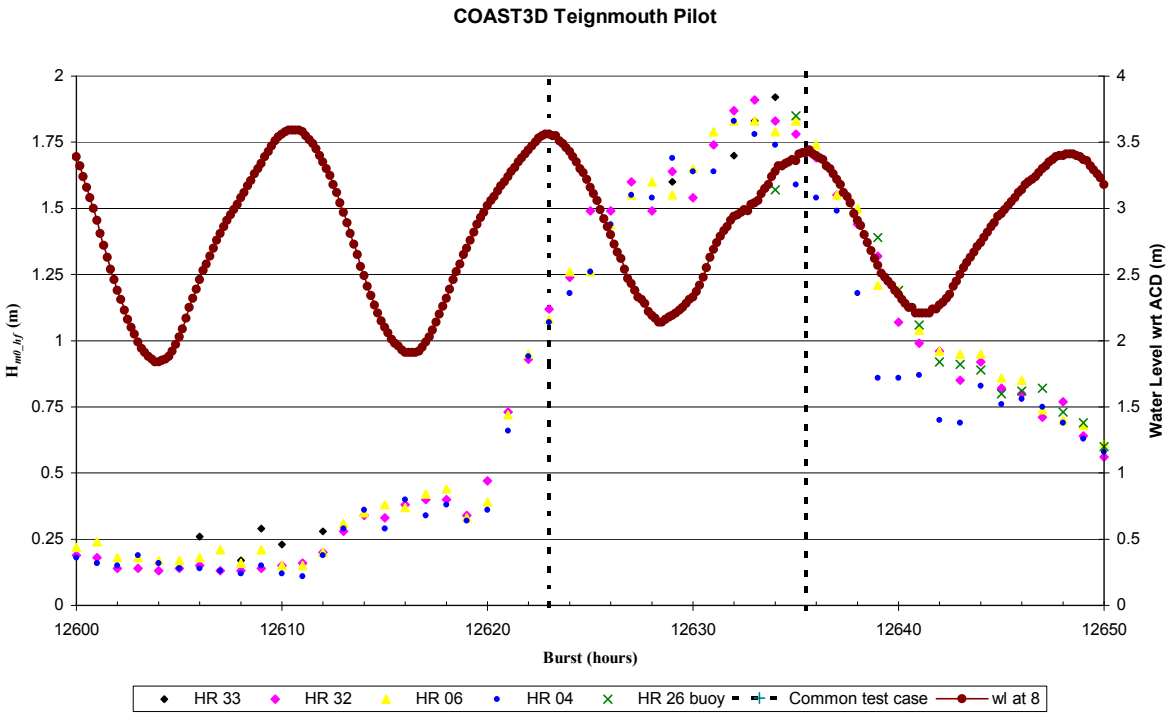

Figure 5. Wave heights and water levels during the near-neap tide plus storm test case.